Dual Functions of SPOP and ERG Dictate Androgen Therapy Responses in Prostate Cancer

Tiziano Bernasocchi[1,2*], Geniver El Tekle[1,2*], Marco Bolis[1*], Azzurra Mutti[1], Arianna Vallerga[1], Laura P. Brandt[3], Filippo Spriano[1,2], Tanya Svinkina[4], Marita Zoma[1,2], Valentina Ceserani[1], Anna Rinaldi[1], Hana Janouskova[1], Daniela Bossi[1], Manuela Cavalli[1], Simone Mosole[1], Roger Geiger[5], Ze Dong[6], Cai-Guang Yang[6], Domenico Albino[1], Andrea Rinaldi[1], Peter Schraml[7], Simon Linder[8], Giuseppina M. Carbone[1], Andrea Alimonti[1], Francesco Bertoni[1], Holger Moch[7], Steven A. Carr[4], Wilbert Zwart[8], Marianna Kruithof-de Julio[3], Mark A. Rubin[3], Namrata D. Udeshi[4], Jean-Philippe P. Theurillat[1+]

[*] These authors contributed equally to this work.

[+]Correspondence to: JeanP_Theurillat@ior.iosi.ch

[1]Institute of Oncology Research, Faculty of Biomedical Sciences, USI, Bellinzona, TI 6500, Switzerland. [2]University of Lausanne, Lausanne, VD 1011, Switzerland. [3]Department of Biomedical Research, University of Bern, 3008 Bern, Switzerland. [4]The Broad Institute of MIT & Harvard, Cambridge, MA 02142, USA. [5]Institute for Research in Biomedicine, Bellinzona, TI 6500, Switzerland. [6]State Key Laboratory of Drug Research, Shanghai Institute of Materia Medica, Chinese Academy of Sciences, Shanghai 201203, China. [7]Department of Pathology and Molecular Pathology, University Hospital Zurich, Zurich, ZH 8091, Switzerland. [8]The Netherlands Cancer Institute, Oncode Institute, 1066CX Amsterdam, Netherlands.

Driver genes with a mutually exclusive mutation pattern across tumor genomes are thought to have overlapping roles in tumorigenesis. In contrast, we show here that mutually-exclusive prostate cancer driver alterations involving the *ERG* transcription factor and the ubiquitin ligase adaptor *SPOP* are synthetic sick. At the molecular level, the incompatible cancer pathways are driven by opposing functions in SPOP. ERG up-regulates wild type SPOP to dampen androgen receptor (AR) signaling and sustain ERG activity through degradation of the bromodomain histone reader ZMYND11. Conversely, SPOP-mutant tumors stabilize ZMYND11 to repress ERG-function and enable oncogenic androgen receptor signaling. This dichotomy regulates the response to therapeutic interventions in the AR pathway. While mutant SPOP renders tumor cells susceptible to androgen deprivation therapies, ERG promotes sensitivity to high-dose androgen therapy and pharmacological inhibition of wild type SPOP. More generally, these results define a distinct class of antagonistic cancer drivers and a blueprint toward their therapeutic exploitation.

Normal cells transform into cancer cells by the acquisition of genetic aberrations in so called driver genes. In some instances, the functional redundancy of mutations in different genes result in a mutually-exclusive mutation pattern across tumor genomes because one alteration is sufficient to activate the specific oncogenic pathway. Based on this assumption, bioinformatic tools have been generated to search for functional redundancy of mutated genes in larger cancer genome data sets[1,2].

In prostate cancer, recurrent gene fusions involving the *ERG* transcription factor and point mutations in the ubiquitin ligase adaptor *SPOP* are two truncal mutations that are mutually exclusively distributed across tumor genomes (Fig. 1a and Supplementary Fig. 1a)[3-7]. The underlying cause for this exquisite pattern remains controversial. While earlier reports suggested a functional redundancy between mutant SPOP and ERG based on the

49 finding that mutant SPOP stabilizes the ERG oncoprotein[8,9], more recent studies challenge
50 this view by showing descriptive evidence for divergence in tumorigenesis[3,10].
51
52 **RESULTS**
53 **Activation of the ERG oncogene and missense mutation in SPOP are synthetic sick**
54 To shed light into the functional relationship of these recurrent driver genes, we
55 assessed the impact of SPOP mutations and ERG activation on the cellular growth of
56 mouse prostate epithelial organoids. To do so, we first established and validated the
57 organoids by the presence of multilayered structure with expression of CK5 and CK8 in
58 basal and luminal cells, respectively (Supplementary Fig. 1b). In agreement with recent
59 reports, lentiviral-transduced point mutants of SPOP (SPOP-Y87C, SPOP-W131G) or a
60 truncated version of ERG, which typically results from gene fusion with androgen-
61 regulated genes in prostate cancer (ΔERG, amino acids 33-486), promoted cell growth (Fig.
62 1b, Supplementary Fig. 1c)[11-14]. While SPOP mutant organoids displayed a round shape,
63 the over-expression of ΔERG gave rise to characteristic finger-like protrusions.
64 Surprisingly, the joint expression of both drivers considerably diminished cell growth and
65 reduced finger-like protrusions, implying a synthetic sick relationship between the two
66 genetic alterations. Cytological follow up analysis revealed reduced proliferation
67 evidenced by reduced Ki-67 and increased p16, P-HP1y positivity and vacuolization of the
68 cytoplasm compatible with senescence induction (Supplementary Fig. 1d).
69 We wondered if the observed synthetic sick relationship also applied to established
70 cancer cells from advanced, castration-resistant metastatic disease. Forced expression of
71 mutant SPOP (SPOP-Y87C, SPOP-W131G) promoted 3D growth of *ERG* fusion-negative

72 LAPC-4 human prostate cancer cells (Supplementary Fig. 2a). The oncogenic effect was
73 paralleled by an increase in the expression of the oncogenic transcription factors MYC and
74 HOXB13 and a decrease in the cell cycle inhibitor p21 as seen also in an organoid line
75 derived from *Spop*^{F133V}-mutant transgenic mice (Supplementary Fig. 2a,b)[11]. In contrast,
76 we observed the opposite phenotypic and molecular changes in VCaP human prostate
77 cancer cells harboring the recurrent *TMPRSS2-ERG* fusion (Fig. 1c, d & Supplementary
78 Fig. 2c, d). In this setting, mutant SPOP (SPOP-Y87C, -F102C, -W131G, -F133S)
79 dramatically decreased the proliferation of cancer cells in culture and the growth of
80 xenograft tumor models *in vivo*. Similarly, to the mouse prostate organoids, induction of
81 senescence was evidenced by an increase of senescence-associated β-galactosidase (SA-β-
82 gal) positive cells and upregulation of p21 and GDF15 protein levels. In line with this, the
83 transfer of conditioned medium from VCaP cells expressing mutant SPOP (SPOP-Y87C ,
84 SPOP-W131G) reduced also the proliferation of parental VCaP cells, indicating a
85 contribution of Senescence-Associated Secretory Phenotype (SASP) to the synthetic sick
86 relationship (Fig. 1d and Supplementary Fig. 2f,j).

87 Conversely, forced expression of ΔERG significantly reduced the growth of SPOP-
88 Y83C mutant LuCaP-147 patient-derived xenograft (PDX) cancer cells *in vivo* and in
89 culture (Fig. 1e, Supplementary Fig. 3a, b)[15], adding orthogonal support for a synthetic sick
90 relationship between mutant SPOP and ΔERG in advanced prostate cancer. In addition,
91 over-expression of MYC promoted cancer cell growth in both VCaP and LuCaP-147 cells
92 (Supplementary Fig. 3c, d). The latter finding may suggest that the over-expression system
93 *per se* is not the underlying cause of the synthetic sick relationship mentioned above.

94 Next, we wondered if genetic or pharmacologic suppression of ERG signaling may

95 revert the growth suppressing function of mutant SPOP in VCaP cells. Indeed, knockdown
96 of ERG by short-hairpin RNA interference decreased the growth of VCaP control cells and
97 of cells over-expressing wild-type SPOP, while it promoted the growth of cells over-
98 expressing SPOP-W131G (Supplementary Fig. 3e). In addition, low doses of the ETS
99 inhibitor YK-4-279 promoted specifically the growth of VCaP cells over-expressing
100 mutant SPOP (Fig. 1f). We noted a similar effect when VCaP cells were co-treated with a
101 small molecule inhibitor of SPOP (Supplementary Fig. 3f)[16]. In aggregate, the data support
102 an antagonistic relationship between oncogenic activation of ERG and a loss of SPOP
103 function in prostate cancer cells.
104

105 **Mutant SPOP-induced androgen receptor signaling antagonizes ERG activity**

106 To assess the underlying molecular biology of the antagonistic relationship between
107 *ERG*-fused and *SPOP*-mutants tumors, we interrogated the transcriptomes from the TCGA
108 cohort to nominate differences across these tumor subtypes. Indeed, the unbiased principal
109 component analysis (PCA) revealed major differences in the transcriptional output (Fig.
110 2a). The differences were maintained in castration-resistant prostate cancers (CRPC) from
111 the (SU2C) cohort using a single-sample gene-set enrichment analysis approach (Fig. 2b).
112 Furthermore, derived (PDX) models also retained analogue transcriptional differences, as
113 demonstrated by different behavior shown by *SPOP*-Mutant (LuCaP-78, -147) and *ERG*-
114 Fused (LuCaP-35, -23.1, VCaP cells) models (Fig. 2b).

115 In *SPOP*-mutant prostate cancer, several dysregulated SPOP substrates (e.g. NCOA3,
116 TRIM24, BET proteins) have been shown to boost the AR pathway leading ultimately to
117 high levels of AR target genes (Supplementary Fig. 4a)[3,11,17-24]. In contrast, *ERG*-fused

118 cancer cells express typically lower levels of AR target genes as illustrated by the widely
119 adopted AR score (Supplementary Fig. 4a)[3]. To get more insights into this different
120 behavior, we further performed differential expression analysis between the two tumor
121 subtypes. Gene-set enrichment analysis resulted in a clear up regulation of the canonical
122 androgen response pathway in *SPOP*-mutant versus *ERG*-fused tumors, as defined by the
123 respective Hallmark gene-set, curated by the Molecular Signature Database (MSigDB)
124 (Supplementary Fig. 4b). In line with the divergence of transcriptome profile identified in
125 the PCA plot of Fig. 2a, a clear division between *SPOP*-mutant and *ERG*-fused tumors was
126 also reported in their respective cistrome counterpart[25]. By re-analyzing ChIP-Seq data, we
127 could determine that most differentially bound regions between both tumor types, are
128 indeed characterized by increased AR-binding in *SPOP*-mutant tumors (Fig. 2c).

129 Next, we analyzed the transcriptome changes of the VCaP cells overexpressing SPOP
130 mutants (SPOP-MTs; SPOP-Y87C, -F102C, -F133S). The unbiased hallmark analysis
131 showed a dramatic increase in the androgen response, recapitulating the changes identified
132 in primary prostate cancer (Supplementary Fig. 4b, 5a and 5b). Based on these results, we
133 posited that differential levels of androgen receptor (AR) signaling in *SPOP*-mutant versus
134 *ERG*-fused cancers might be at the root of the incompatibility between the driver events.
135 Thus, we analyzed in particular AR- and ERG-related transcription in VCaP cells, and
136 generated a custom signatures using ChIP-seq data and matched RNA-seq samples
137 (Supplementary Table 1)[25]. As expected, SPOP-MTs increased the transcription of genes
138 bound by AR and induced by its ligand dihydrotestosterone (DHT), whereas genes bound
139 by AR and repressed by DHT were further reduced (Fig. 3a, Supplementary Fig. 5c, and
140 Supplementary Table 1). Remarkably, we observed the opposite effect on genes bound

141 only by ERG. Mutant SPOP downregulated ERG-induced genes (e.g. MYC) and
142 upregulated ERG-repressed genes, respectively (Fig. 1d). In line with these findings, gene
143 ontology analysis of AR-ERG co-bound gene signature in VCaP cells indicated that the
144 most striking transcriptional changes were linked to cellular differentiation and cell cycle
145 arrest that are directly induced by DHT and repressed by ERG (e.g. HOXA genes,
146 CDKN1A/p21, Fig. 1d, Fig. 3b, Supplementary Fig. 5d). To reduce the number of genes
147 falling within our custom signatures, we used a particularly restrictive approach and
148 considered as co-bound only genes where AR and ERG binding sites were overlapping for
149 at least 1bp. As a result, some genes (i.e. CDKN1A/p21) which are bound both by AR and
150 ERG in their promoter region, but which bindings do not overlap, are not included in this
151 category despite being bona fide co-bound targets.

152 The dramatic upregulation of this gene set was paralleled by a downregulation of cell
153 cycle genes (e.g. E2F and MYC targets), implying a direct link between the induction
154 AR/ERG co-bound genes, the repression of ERG targets, cell differentiation and the
155 synthetic sick relationship of ERG and mutant SPOP (Fig. 1d, Supplementary Fig. 5a-e).
156 The relationship of AR- and ERG-related custom signatures to the hallmark gene sets are
157 highlighted in Fig. 3c in a two-dimensional network. Moreover, independently generated
158 signatures of senescence-associated transcripts were enriched in VCaP overexpressing
159 SPOP mutants, further corroborating our data of a senescence-induced cell cycle arrest (
160 Supplementary Fig. 5f)[26,27].

161 Conversely, we assessed the consequence of ERG over-expression in LNCaP cells
162 under low DHT levels where mutant SPOP triggers AR signaling and tumor growth
163 (Supplementary Fig. 6a,b)[17,21]. Over-expression of ΔERG in this setting robustly reverted

164 the induction of signatures related to cell proliferation (e.g. E2F and MYC targets) and AR
165 signaling. Taken together, the data implies a reciprocal incompatibility of mutant SPOP
166 induced AR signaling and the function of the ERG oncogene.

167 Next, we verified if corresponding transcriptional changes were found in clinical tissue
168 samples. Indeed, ERG-regulated genes culled from VCaP cells were up-regulated in *ERG*-
169 fused and down-regulated in *SPOP*-mutant primary tumors (Fig. 3d, Supplementary Fig.
170 4c)[3]. Importantly, the most striking changes between the two groups were found again in
171 the AR/ERG co-bound gene set in primary prostate cancers (Supplementary Fig. 4d)[3,6].
172 The results underscore both the relevance of our cell culture-based data and highlight the
173 transcriptional differences among *ERG*- and *SPOP*-driven tumors.

174

175 **ZMYND11 is a *de novo* SPOP substrate**

176 Using tandem mass tag (TMT)-based quantitative mass-spectrometry, we set out to
177 search for SPOP substrates that may influence the activity of AR and ERG and thereby
178 may cause to the synthetic sick relationship between mutant SPOP and ERG in VCaP cells
179 overexpressing mutant SPOP (SPOP-MTs; SPOP-Y87C, -F102C, -W131G, Fig. 4a).
180 Because recurrent loss-of-function SPOP mutants impair substrate ubiquitylation and
181 proteasomal degradation, we searched for proteins which expression levels increase
182 without concomitant increase in mRNA levels (Fig. 4b, Supplementary Fig. 7a). Overall,
183 we noted a strong correlation of protein with mRNA expression changes with consistent
184 changes of our AR and ERG custom signatures at the protein level (Fig. 4b, Supplementary
185 Fig. 7b, c). In addition, we found a marked upregulation of the known SPOP substrate and
186 AR activator TRIM24 at the protein level (Fig. 1d & 4a, Supplementary Table 2)[20,21] and

187 subsequently assessed if TRIM24 and more generally AR is implicated in the synthetic
188 sick relationship between mutant SPOP and ERG. Indeed, knockdown of TRIM24 by two
189 short hairpin RNAs partially reverted the growth inhibition mediated by mutant-SPOP in
190 VCaP cells and reduced AR signaling (Supplementary Fig. 7d-f), while over-expression of
191 AR was sufficient to decrease cellular growth (Supplementary Fig. 7g, h).

192 The most striking upregulation was noted for the bromodomain histone reader
193 ZMYND11 (Fig. 4b). In line with a SPOP substrate, wild type SPOP bound and decreased
194 the expression of HA-ZYMND11 in a proteasome-dependent manner (Fig. 4c, d). We
195 found two degron sequences that were required for efficient SPOP-mediated ubiquitylation
196 and protein degradation (Fig. 4e-g, Supplementary Fig. 8a.). As expected, SPOP mutants
197 failed to bind and adequately ubiquitylate HA-ZMNYD11-WT (Fig. 4h-j)[8,9,18-20,22-24].
198 Finally, we confirmed that expression of mutant SPOP prolonged the half-life of
199 endogenous ZMYND11 in VCaP cells and upregulated ZMYND11 expression in other
200 prostate cancer cells (Fig. 4k and Supplementary Fig. 8b).

201

202 **ZMYND11 induces AR signaling pathway and represses ERG activity**

203 Next, we assessed if ZMYND11 protein upregulation also contributed to the synthetic
204 sick relationship. In support, forced expression of the degron-deficient variants of
205 ZMYND11 (HA-ZMYND11-DMT1/DMT2) was sufficient to diminish the growth of
206 VCaP cells (Fig. 5a, b, Supplementary Fig. 8c), while knockdown of ZMYND11 partially
207 reverted the growth inhibition mediated by mutant SPOP (Fig. 5c).

208 We postulated that ZMYND11 up-regulation could contribute to the synthetic sick
209 relationship by repressing the transcriptional activity of the ERG oncogene or enhancing

210 AR signaling. To this end, expression changes induced by HA-ZMYND11-DMT2 largely
211 overlapped with genes perturbed by mutant SPOP while the opposite was noted when
212 ZMYND11 expression was reduced by RNA interference (Fig. 5d and Supplementary Fig.
213 8d). In comparison to mutant SPOP, AR and ERG target genes were similarly dysregulated
214 by HA-ZMYND11-DMT2 (Fig. 5e). Because the PWWP domain of ZMYND11 has been
215 involved in the regulation of transcription through its ability to bind H3K36me3 histone
216 marks[28], we tested the contribution of this domain to the overall transcriptional output.
217 Indeed, the PCA of VCaP cells over-expressing either HA-ZMYND11-DMT2 or a PWWP
218 domain deficient mutant (W294A) revealed a major contribution of this domain to the
219 ZMYND11 induced transcriptional changes (Supplementary Fig. 8e).

220 Subsequently, we mapped the genomic occupancy of ZMYND11 in VCaP cells
221 expressing the SPOP-Y87C mutant by chromatin immunoprecipitation sequencing (ChIP-
222 seq) and found an enrichment of ZMYND11 binding sites at promoter regions controlling
223 ERG-induced genes (e.g. MYC,) and AR/ERG co-bound genes (e.g. p21/CDKN1A) (Fig.
224 5f, g and Supplementary Fig. 9a-e). The data imply a critical enhancer function of
225 ZMYND11 in boosting AR signaling and repressing ERG signaling downstream of mutant
226 SPOP.

227

228 **Wild type SPOP is required for ERG oncogenic function**

229 We reasoned that ERG-driven tumors might require wild type SPOP to degrade
230 ZMYND11 and thereby unlock the oncogenic function of ERG. In support, over-
231 expression of wild type SPOP increased the 3D growth of mouse prostate epithelial
232 organoids and VCaP cells only when ERG was over-expressed (Fig. 1b, Supplementary

233 Fig. 2c, 10a, b). Remarkably, ERG-fused human tumor tissues displayed also the highest
234 SPOP mRNAs levels (Fig. 6a). Thus, we wondered if ERG itself may directly upregulate
235 SPOP transcription to support its own oncogenic activity. Indeed, mining ERG ChIP-seq
236 data in VCaP cells revealed ERG bindings sites in the promoter region of SPOP
237 (Supplementary Fig. 10c). Moreover, knockdown of ERG reduced SPOP protein levels in
238 VCaP cells, while forced expression of a ΔERG led to the upregulation of SPOP mRNA
239 and protein levels in PC3 cells (Fig. 6b, Supplementary Fig. 3e, and 10d).

240 We then asked if the elevated SPOP levels in the context of forced ΔERG expression
241 have a functional impact on the oncogenic activity of ΔERG in the androgen-independent
242 PC3 cells, in which ERG promotes tumor cell invasion[29]. Indeed, the reduction of SPOP
243 levels by RNA interference reduced the ability of ΔERG to invade into matrigel (Fig. 6c).
244 Similarly, knockdown of SPOP in VCaP cells reduced cell growth in 3D cell culture and
245 impaired ERG-mediated gene transcription (Supplementary Fig. 10e, f). In accordance
246 with the ability of mutant SPOP to repress the function of endogenous wild type SPOP in
247 a dominant-negative manner, the over-expression of mutant SPOP (SPOP-Y87C, -F102C,
248 -W131G, -F133S) phenocopied the effect of SPOP knockdown on ERG-mediated invasion
249 in PC3 cells (Supplementary Fig. 10g, h). In agreement with the established repressive
250 function of ZMYND11 on ERG, we found that over-expression of HA-ZMNYD11-DM2
251 was sufficient to repress ERG-induced invasion and established target genes in PC3 cells
252 (Fig. 6d, e). Taken together, the data imply the existence of a positive feed-forward loop,
253 in which ΔERG promotes the expression of SPOP to sustain its oncogenic activity.
254

255 **ERG and mutant SPOP trigger different responses to therapeutic interventions**

256 Based on the above-mentioned differences in tumorigenesis, we speculated that ERG
257 or mutant SPOP could also trigger different therapeutic responses. In light of the
258 dependency of ERG-driven tumors on wild type SPOP function, we hypothesized that
259 *ERG*-fusion positive cells may be particularly sensitive to pharmacological inhibition of
260 SPOP. We analyzed the response of the SPOP small molecule inhibitor compound 6b
261 (SPOP-i) in *ERG*-fused, *SPOP* mutant and other prostate cancer cell lines and patient-
262 derived xenograft models (PDX)[16]. The SPOP inhibitor increased the protein but not the
263 mRNA levels of established SPOP substrates and ZMNYD11 while the related inactive
264 analog compound 6c did not (Supplementary Fig. 11a-c). The latter did also not exert any
265 activity in 3D culture models (Supplementary Fig. 11d). In agreement with our previous
266 results, we found that *ERG*-fused cells (VCaP, LuCaP-23.1, -35) were more sensitive to
267 SPOP-i than *ERG*-negative cells (22Rv1, LNCaP, PC3), while *SPOP* mutant cells (LuCaP-
268 78, -147) were particularly insensitive in 3D culture models and in xenograft tumor models
269 *in vivo* (Fig. 7a-f, Supplementary Fig. 11e). We further validated our results in the mouse
270 prostate epithelial organoids and confirmed the increased sensitivity of ΔERG-expressing
271 cells to SPOP inhibition in this isogenic system (Fig. 7g).

272 Given the notion that wild type SPOP dampens AR function in the context of ERG to
273 sustain tumor growth, we asked if VCaP cells are particularly susceptible to increased DHT
274 levels. Indeed, exposure to high-dose of testosterone *in vivo* or DHT *in vitro* induced
275 similar molecular changes as for the over-expression of mutant SPOP and greatly
276 suppressed the growth of *ERG*-fusion positive cells but not of *SPOP* mutant cells *in vitro*
277 and *in vivo* (Fig. 1c, 8a-f and Supplementary Fig. 12a-e). Moreover, signatures of
278 senescence-associated transcripts were also enriched in VCaP cells upon treatment with

279 DHT, further corroborating our data of a senescence-induced cell cycle arrest
280 (Supplementary Fig. 12f). Strikingly, the sensitivity to SPOP-i and to high testosterone *in*
281 *vivo* correlated well with ERG protein expression levels in the respective ERG-fusion
282 positive cell line and PDX model (Fig. 8g, h). The data suggests a therapeutic opportunity
283 for SPOP inhibition or high-dose androgen therapy in prostate cancers that express high
284 levels of ERG.

285 Conversely, and because *SPOP* mutant cancers are driven predominantly by androgen
286 signaling and consequently display high-level activation of AR-related transcripts in
287 human tumor tissues, we speculated that these tumors may be particularly susceptible to
288 androgen deprivation or anti-androgen therapies (ADT) (Supplementary Fig. 4c). Indeed,
289 the prevalence of *SPOP* mutations in primary tumors -and tumors that had progressed after
290 initial surgery or radiotherapy- is consistently higher as compared to tumors that had
291 become resistant to subsequent ADT (also referred as castration-resistant prostate cancer,
292 CRPC, Supplementary Fig. 13a). In line with the notion that this difference may be related
293 to a better response of SPOP mutant tumors to ADT, SPOP mutant tumor display a trend
294 towards better overall survival despite progressing faster after initial therapy (Fig. 9a,b).
295 To functionally analyze the response of androgen deprivation or the anti-androgen
296 enzalutamide, we chose to ectopically expressed different SPOP variants and ΔERG in the
297 androgen-dependent human LAPC4 prostate cancer cells that are wild-type for both driver
298 genes. In accordance with the clinical observation, the presence of mutant SPOP (SPOP-
299 Y87C, SPOP-W131G) rendered LAPC4 cells more susceptible to either ADT or
300 enzalutamide in comparison to cells expressing control vector (Fig. 9c, Supplementary Fig.
301 13b). In contrast, ΔERG rendered the same cells more resistant to enzalutamide. In line

302 with the previous findings in VCaP and LuCaP-147 cells, ΔERG expression rendered
303 LAPC4 cells susceptible to high levels of DHT, while mutant SPOP had the opposite effect
304 (Supplementary Fig. 13b). Taken together, the different responses to established and
305 experimental therapeutic modalities observed between mutant SPOP and ERG add further
306 credence to their divergent roles of the AR pathway related to tumorigenesis.
307

308 **DISCUSSION**

309 Although multiple studies over recent years have uncovered different genetically-
310 defined subtypes of primary prostate cancer, their biological understanding and therapeutic
311 implications remain largely unexplored territory. Here, we report two diametrically
312 different paths toward tumorigenesis triggered by either highly recurrent missense
313 mutation in *SPOP* or gene fusion involving the *ERG* oncogene. Importantly, wild type
314 SPOP emerges as a critical component that enforces oncogenic ERG signaling in part
315 through dampening AR activity, while mutant SPOP drives tumorigenesis through
316 activation of AR signaling. Moreover, several studies have previously highlighted the
317 importance of AR target genes in the context of SPOP mutants and ERG positive tumors
318 [17,30,31]. Based on the incompatibility between the two tumor subtypes, our work enabled
319 the development of specific custom signatures related to AR and ERG transcript that are
320 necessary to drive proliferation and tumorigenesis in the context of *ERG*-positive and
321 *SPOP*-mutants tumors. In addition, we show that the bromodomain histone reader
322 ZMYND11 is a SPOP substrate implicated downstream of SPOP in the opposing
323 regulation of the ERG and AR pathway in the two tumor subtypes (Fig. 10). The AR and
324 ERG pathways have been previously reported to have a partially antagonistic

325 relationship[31,32], further corroborating our findings.

326 Because activation of the androgen receptor by androgens represents a key lineage
327 specific oncogenic pathway in prostate cancer, androgen deprivation/antagonization
328 therapies (ADT) remain the uniform treatment modality up to this very day. That said, the
329 responses to ADT are highly variable and may last from a few weeks up to many years.
330 Here, we provide functional evidence that pre-existing prostate cancer founder mutations
331 influence the treatment response. Most notably, *SPOP* mutations promote susceptibility to
332 androgen deprivations therapies. In agreement with our findings, earlier reports have
333 shown underrepresentation of *SPOP* mutant tumors in cohorts of castration-resistant
334 disease and a more favorable response to the abiraterone and enzalutamide[33,34].

335 Conversely, we show that the presence of the ERG oncogene increases the
336 susceptibility of tumor cells to high-dose androgen therapy, while cells expressing mutant
337 SPOP remain largely unaffected. This is of clinical interest because testosterone treatment
338 of patients with advanced castration-resistant disease has recently shown to trigger anti-
339 tumor responses in around one third of the patients[35]. It is tempting to speculate that these
340 insights may help to discern responders from non-responders.

341 In addition, we provide evidence that the antagonistic relationship between mutant
342 SPOP and ERG may be used towards the development of new therapeutic avenues. More
343 specifically, we show that ERG-driven cancer cells are particularly sensitive to the
344 inhibition of wild-type SPOP using recently developed small molecule inhibitors[16]. Our
345 preclinical data suggests that SPOP inhibition may be effective in clinical settings where
346 ERG is robustly expressed (e.g. neo-adjuvant setting or early metastatic disease).

347 More generally, our results identify another paradigm for antagonistic driver genes in

348 prostate cancer that has recently emerged also for other cancer types [36-38]. In analogy to
349 prostate cancer, truncal point mutations in *DNMT3A* and gene fusions in *PML-RARA* are
350 mutually exclusive drivers in acute myeloid leukemia (AML). Similarly to SPOP, intact
351 DNMT3A has been found to be critical for PML-RARA-driven leukemia (Supplementary
352 Fig. 14a, b) [39,40]. Importantly, we demonstrate here for prostate cancer that the concept of
353 antagonistic driver genes can be exploited to identify therapeutic opportunities.
354

355 **Acknowledgements**

356 We thank the University of Washington and Eva Corey and Donna M. Peehl for
357 providing the Patient-Derived Xenografts (PDX) models. We thank Martina Storz,
358 Susanne Dettwiler, Carmen Gavrisan, and Christiane Mittmann for histology assistance.
359 We thank Enrica-Mira Catò and all members of the IOR/IRB animal core facility for
360 technical assistance and the animal work. In addition, we thank all member of the
361 laboratory for scientific discussions. The results shown here are in whole or part based
362 upon data generated by the TCGA Research Network: https://www.cancer.gov/tcga. J.P.T
363 is funded by a Swiss National Science Foundation Professorship (PP00P3_150645 &
364 PP00P3_179072) grant, and grants by the Swiss Cancer League, the Lega Ticinese contro
365 il cancro, and the Fidinam Foundation. This work was also supported in part by grants from
366 the National Cancer Institute (NCI) Clinical Proteomic Tumor Analysis Consortium grants
367 NIH/NCI U24-CA210986 and NIH/NCI U01 CA214125 (to S.A.C.).
368

369 **Author Contributions**

370 T.B. and J.P.T. originally developed the concept, further elaborated on it and designed

371 the experiments together with G.E.T. and M.B. ; T.B. and G.E.T. performed experiments
372 and analyzed the data together with N.D.U., S.A.C., A.M., T.S., L.P.B., F.S., M.Z., V.C.,
373 Anna R., H.J., D.B., M.C., D.A. and R.G.. T.B. and G.E.T. performed xenograft tumor
374 experiments in immunodeficient mice. Z.D. and C.G.Y. provided SPOP 6b and SPOP 6c
375 compounds. M.S. , S.D. and S.M. performed immunohistochemical experiments and J.P.T
376 the subsequent analysis. H.M. and P.S. provided prostate cancer samples. M.B., A.V. and
377 Andrea R. analyzed genomic and RNA-Seq data. J.P.T, H.M., S.A.C., M. A. R., M.K.J.,
378 A.A., F.B., W.Z. and G.M.C provided funding and resources. J.P.T., T.B., G.E.T. and M.B.
379 interpreted the data and wrote the paper. T.B., G.E.T. and M.B. contributed equally to this
380 work.
381

382 **Author Information**

383 MAR is listed as a co-inventor on US and International patents in the diagnostic and
384 therapeutic fields of ETS gene fusion prostate cancers (Harvard and University of
385 Michigan) and SPOP mutations (Weill Cornell Medicine). JPT has received funding for
386 the venue of scientific conferences from Astellas, MSD, and Janssen/Cilag. The remaining
387 authors declare no competing financial interests. Correspondence and requests for
388 materials should be addressed to J.P.T. (JeanP_Theurillat@ior.iosi.ch)
389

390 **Methods**

391 **Cell culture, Transfection and Infection**

392 VCaP, LNCaP, PC3, 22Rv1, HEK293 cells were purchased from ATCC. LAPC-4 were a
393 gift from Prof. Helmut Klocker. VCaP and HEK293 were grown in DMEM with Glutamax

394 (Gibco); LNCaP, PC3, 22Rv1, LAPC-4 in RPMI medium (Gibco); all were supplemented
395 with 10% full bovine serium (FBS; Invitrogen), or 10% charcoal-stripped serum (CSS;
396 One Shot Fetal Bovine Serum, Charcoal Strippped, Gibco) for androgen deprivation
397 therapy response, and 1% Penicilin/Streptomycin. LuCaP-147 were grown in StemPro
398 medium (hESC SFM StemPro, Gibco) with regular supplements. All cells were incubated
399 at 37°C and 5% CO_2 and routinely tested for mycoplasma contamination.
400 For stable knockdown experiments, cells were infected with pLKO-1 vectors (Sigma) and
401 the following clones were used; *SPOP*: TRCN0000140431 (shSPOP_1) and
402 TRCN000013911 (shSPOP_2); *TRIM24*: TRCN000021262 (shTRIM24_1) and
403 TRCN0000195528 (shTRIM24_2); *ERG*: TRCN0000429354 (shERG_1) and
404 TRCN0000432394 (shERG_2); *ZMYND11*: TRCN0000275479 (shZMYND11_1) and
405 TRCN0000275542 (shZMYND11_2). After infection, cells were selected in the presence
406 of puromycin (2 μg/ml).
407 For SPOP, ΔERG, HA-ZMYND11-WT, HA-ZMYND11-DMT1, HA-ZMYND11-DMT2,
408 MYC and AR over-expression a derivate of the pLX304 vector was used throughout in
409 which the CMV promoter has been exchanged to a PGK promoter and the blasticidin
410 cassette left unchanged (ΔERG constructs) or exchanged by a puromycin resistance
411 cassette (SPOP constructs) (pLX_TRC_307, available at Addgene as Plasmid 41392,
412 pCW107). All ORFs were cloned into pLX_TRC_307 using Nhe1 and Mlu1. Tumors from
413 PDX LuCaP-78, -147, -35,-23.1 were collected, dissociated and cultured as previosly
414 described[41].

415 **Chemicals**

416 MG-132 (M7449) and Cycloheximide (CHX, C4859) were purchased from Sigma and
417 used at 20 μM and 100 μg/ml in all experiments, respectively. SPOP inhibitor (SPOP-i,
418 compound 6b) and its inactive analog (compound 6c), were provided by the laboratory of
419 C. Yang (State Key Laboratory of Drug Research, Shanghai Institute of Materia Medica).
420 DHT (5α-Dihydrotestosterone) was purchased from Sigma (D-073), MDV3100
421 (Enzalutamide) was purchased from APExBIO (A3003). YK-4-279 (ETS inhibitor) was
422 purchased from Selleckchem. All chemicals were used at the indicated concentration.
423

424 **Dose-response curves and cell-growth assays**

425 Cells were seeded (between $1x10^3$ and $1x10^4$ per well) in a 96-well plate. Cells were
426 subsequently treated with serial dilutions of DHT (in 10% CSS medium), or enzalutamide;
427 SPOP inhibitor, ETS inhibitor to determine dose-response curves or were left untreated for
428 cell-growth assays. Proliferation at corresponding time points was assessed by MTT
429 (Methylthiazolyldiphenyl-tetrazolium bromide) assay according to the manufacturer's
430 recommendations (Sigma). For each time point, absorbance (OD, 590 nm) was measured
431 in a microplate reader.
432

433 **SA-β-galactosidase staining of VCaP cells**

434 Senescence-associated-β-galactosidase (SA--β-gal) staining was performed using the
435 Senescence β-Galactosidase Staining Kit (Cell Signaling, #9860) following the
436 manufacturer's instructions. To avoid false-positive staining, we adapted the β-
437 Galactosidase Staining Solution to pH 7. Cells incubated with glycerol 70% were observed
438 under a bright field microscope.

439

440 **Matrigel Invasion assay**

441 Invasion assay was performed as previously described[42]. Briefly, equal number of PC3
442 cells were seeded into 10cm dishes and starved with a medium without fetal bovine serum
443 for 24 hr.; subsequently $1x10^5$ cells were resuspended in 100 µl of starved medium and
444 seeded onto the basement of a Boyden chamber (CLS3422; Sigma) coated with Matrigel.
445 RPMI with 10% fetal bovine serum was added to the lower chamber. After 48hr, invaded
446 cells were fixed with 10% of formalin and stained with crystal violet. Absorbance was
447 measured at 560 nm**.**

448 **Clonogenic assay in methylcellulose**

449 Cells were seeded (between $5x10^3$ and $1x10^4$) in methylcellulose (Methocult H4100,
450 StemCell Technologies) in triplicate. Cells were left untreated for cell-growth assay. For
451 SPOP inhibitor assay, cells were treated with vehicle (0.1% DMSO) or drug (SPOP-i) at
452 corresponding concentration. For androgen therapy, cells were treated with vehicle (0.01%
453 Methanol) or DHT at corresponding concentration. Cells were incubated at 37°C and 5%
454 CO_2 for 7-28 days and colonies were stained with MTT solution at 37°C overnight and
455 absorbance (OD, 590 nm) was measured in a microplate reader.

456

457 **Mouse Prostate Organoid Generation and Experiments**

458 Prostate tissue was extracted from euthanized mice, digested and seeded in matrigel as
459 previously described[43]. To overexpress *SPOP* species and *ΔERG* genes, mouse prostate
460 cells were virally infected by spinoculation for 1hr at 600g at 32 °C and selected with

461 puromycin. For the ‘‘organoid formation assay’’ $1.5x10^4$ single cells were plated per well
462 onto 40µl of Matrigel on day 1 and organoids were grown in “revised human prostate
463 organoids medium” as previously described[41]. Briefly, the medium included the following
464 reagents: adDMEM/F12, glutaMAX (2mM), Pen-strep 100u/ml, HEPES (10mM), B27
465 (1X), EGF (5ng/ml), AB3-01 (500nM), Noggin (100ng/ml), R-Spondin 1 (500ng/ml),
466 DHT (1nM), FGF-2 (5ng/ml), FGF-10 (10ng/ml), Prostaglandin E2 (1000nM). The
467 number of formed organoids that reached 100 µM of diameter was counted on days 14 post
468 plating with cellSens software (Olympus). For the Dose-Response experiment $1x10^4$
469 mouse prostate cells were plated in 40µl of Matrigel and treated with vehicle (0.1% DMSO)
470 or drug (SPOP-i) at indicated concentration for 7 days. Live/dead staining was performed
471 using Calcein AM (final concentration 1uM) and Ethidium Homodimer I (EthD-1, final
472 concentration (1.33uM) dissolved in the medium for 1 hour. GFP or RFP positive
473 organoids were analyzed under a fluorescence microscope. The percentage of dead
474 organoids (RFP positive) was normalized to the Etoposide-treated (positive control)
475 organoids. The genetically engineered Mouse Prostate Organoids, derived from
476 PbCre;$R26^{F133V}$, were generated as previously described[11].
477

478 **Immunohistochemistry**

479 Cytoblocks were prepared from the pellets of organoids by adding plasma and thrombin in
480 order to obtain a solid matrix. Once solidified, the organoids were fixed in 10% formalin
481 (Thermo Scientific, 5701) and embedded in paraffin as a normal tissue. Sections of 4 µm
482 were used for IHC analyses and hematoxylin and eosin (H&E) staining (Diapath, C0303)
483 and (Diapath, C0363) respectively. Once dried the sections were treated with OTTIX plus

484 solution (Diapath, X0076) and OTTIX shaper solution (Diapath, X0096) to dewax and
485 rehydrate the sections. Antigen retrieval was performed using pH 6 solutions at 98°C for
486 20 min. Successively the endogenous peroxidases and non-specific binding sites were
487 blocked using 3% H2O2 (VWR chemicals, 23615.248) and Protein-Block solution (DAKO
488 Agilent technologies, X0909) respectively, for 10 min. Sections were then stained for anti-
489 p16 (ab211542, Abcam, 1:1200), anti-Ki67 (Clone SP6; Lab Vision Corporation #RT-
490 9106-R7, RTU) anti-Phospho-HP1y (Ser83) Antibody (CST #2600, 1:200), anti-CK8
491 (ab,59400, Abcam), anti-CK5 (ab52635, Abcam). IHC analyses were performed using the
492 Imagescope software.
493
494 ***In vivo* experiments**
495 All animal experiments were carried out in male athymic nude mice (Balb/c nu/nu, 6-
496 8 weeks old), NSG mice (NOD Scid Gamma, 6-8 weeks old), and NRG (NOD Rag gamma,
497 6-8 weeks old) accordingly to protocol approved by the Swiss Veterinary Authority (No.
498 TI-14-2014, TI-38-2018, TI-39-2018 and TI-42-2018). Patient-derived xenografts (PDX)
499 LuCaP-147, -78, -35, -23 were provided by Eva Corey (University of Washington) and
500 maintained as previously described[44]. $2x10^6$ VCaP cells, $5x10^6$ LuCaP-147, LuCaP-23.1,
501 LuCaP-35 and LuCaP-78 were resuspended in 100 µl of PBS and Matrigel 1/1 and
502 subcutaneously injected into both of the dorsal flanks of the mice. Tumor growth was
503 recorded using digital caliper and tumor volumes were calculated using the formula ($L \times W$
504 $^2) /2$, where L=length and W=width of tumor. For the testosterone propionate (25mg/kg)
505 and SPOP inhibitor (SPOP-i, 50mg/kg) treatment, the mice were grouped randomly and
506 the treatment started when the mean tumor volume reached $100m^3$. Tumor volume and

507 weight were measured 2 times per week. Testosterone propionate was resuspended first in
508 ethanol (150mg/kg) and then in Corn oil (Sigma) at a final concentration of 25mg/kg. SPOP
509 inhibitor was resuspended in Dulbecco's phosphate buffered saline (PBS) at a final
510 concentration of 50 mg/kg. At the end of the experiment, mice were euthanized, tumors
511 extracted and weighted. Testosterone level was measured using the Human Testosterone
512 ELISA Kit from Abcam (ab174569). In order to recapitulate the levels of
513 supraphysiological testosterone administrated in clinical trials[35], mice reaching at least 3
514 times the testosterone levels measured before the treatment initiated were included in the
515 depicted data.

516 **Antibodies, Immunoblotting, and Immunoprecipiation**

517 Antibodies used in immunoblotting and immunoprecipitation assays were: anti-SPOP
518 (ab81163, Abcam), anti-TRIM24 (Sc-271266, Santa Cruz), anti-ß-ACTIN (4967, Cell
519 Signaling), anti-AR (Sc-7305, Santa Cruz), anti-GADPH (Sc-47724, Santa Cruz), anti-
520 ERG (Sc-271048, Santa Cruz), anti-α-Tubulin (3873S, Cell Signaling), anti-ZMYND11
521 (NBP2-20960, Novus Biologicals), anti-HA (H3663, Sigma), anti-BRD2 (A302-583A,
522 Bethyl Labs), anti-NCOA3 (2126, Cell Signaling), anti-DEK (610948, BDBioscience),
523 anti-p21 (2947S, Cell Signaling) , anti-c-MYC (5605S, Cell Signaling), anti-HOXB13 (Sc-
524 28333, Santa Cruz), anti-PTEN (9559, cell signaling), anti-p21 (ab188224, Abcam), anti-
525 HOXB13 (NBP2-43655, Novus biologicals), anti-GDF-15 (27455-1-AP, proteintech). All
526 antibodies were employed at dilutions suggested by the manufacturers.

527 For immunoblotting, cells were washed with PBS and subsequently lysed in RIPA
528 buffer (Sigma) and sonicated. Protein concentration was determined using the BCA reagent
529 (ThermoFisher), same amounts of protein were separated by SDS-PAGE (Biorad) and

530 transferred onto PVDF membrane (ThermoScientific). The membrane was incubated for
531 one hour in 5% nonfat dry milk/TBS-T blocking buffer followed by incubation with the
532 primary antibody overnight at 4°C. The membrane was washed with TBS-T followed by
533 incubation with horseradish peroxidase-conjugated secondary antibody (Promega).

534 To detect interactions of SPOP and ZMYND11, cells were lysed in 1 % NP40 buffer
535 (50mM Tris-HCl pH 7.4, 150 mM NaCl, 1 % NP40) with 2x protease inhibitor cocktail
536 (Complete, Roche), sonicated, and 3 mg of lysate were incubated overnight with 2 μg of
537 anti-HA-tag or control mouse IgG antibody (sc-2025, Santa Cruz Biotechnology) at 4 °C.
538 Subsequently, antibodies were collected by 25 μl protein A/G magnetic beads (88803,
539 Fisher Scientific) for 2h, followed by 2 washing steps with 1 % NP40 buffer. Proteins were
540 eluted by addition of 1x SDS-sample buffer under reducing conditions at 95 °C for 5 min.

541 ***In Vivo* Ubiquitylation Assay**

542 293T cells were transiently transfected with indicated plasmids: pCW107-HA-ZMYND11-
543 WT or HA-ZYMND11-DMT1/DMT2 (2 μg), pCW107-SPOP-WT or SPOP-MT (2 μg),
544 CMV-8x Ubi-His (2 μg). 42 hours later, cells were treated with MG-132 (20μM) or DMSO
545 for additional 7 hours. Cells were then washed with PBS and collected by centrifugation.
546 Small amount of cells was lysed in RIPA buffer and the rest in Buffer C (6M guanidine –
547 HCL, 0.1 M Na2HPO4/NaH2PO4, 10mM Imidazole, pH=8). The whole cells extract was
548 sonicated and incubated with 60 μl of Ni-NTA agarose (Sigma) overnight at 4°C. Next,
549 Ni-NTA beads were washed once with Buffer C, twice with Buffer D (1 volume of Buffer
550 C: 3 volumes of Buffer E) and once with Buffer E (25 mMTris-HCL, 20 mM Imidazole,
551 pH=6.8). Elution of bound proteins was processed by boiling in 1x SDS loading buffer

552 containing 300 mM Imidazole. Samples were loaded, separated by SDS-PAGE, and
553 detected by immunoblotting.

554

555 **Gene Expression Studies**

556 RNA was extracted using the RNeasy kit (Qiagen) and processed by Kapa SybrFAST
557 one-Step qRT-PCR kit according to manufacturer`s instructions. qRT-PCR was undertaken
558 on an Applied Biosystems StepOnePlus System. The target mRNA expression was
559 quantified using ΔΔCt method and normalized to Actin expression. The following primers
560 were used: *SPOP*, forward 5'- GAAATGGTGTTTGCGAGTAAACC-3', reverse 5`-
561 TACCTACGCTTCCAGTCTCTG-3'; *ERG*, forward 5'-
562 TGTATGCCAGCATTTGTTTCTT-3', reverse 5'- TTGCTGGTCTTGCCATTCCT-3';
563 *β-ACTIN,* forward 5'-AAGGAGCCCCACGAAAAAT-3', reverse 5'-
564 ACCGAACTTGCATTGATTCCAG-3'; *PLAU,* forward 5'-
565 TACGGCTCTGAAGTCACCACCAAAAT-3', reverse 5'-
566 CCCCAGCTCACAATTCCAGTCAA-3'; *PLAT,* forward 5'-
567 CACTGGGCCTGGGCAAACATA-3', reverse 5'-CACGTCAGCCTGCGGTTCTTC-3';
568 *TMPRSS2,* forward 5'-CAGGAGTGTACGGGAATGTGATGGT-3', reverse 5'-
569 GATTAGCCGTCTGCCCTCATTTGT-3'; *KLK2*, forward 5'- CTGCCCATTGCCTAA
570 AGAAG-3', reverse 5'- GTAGAGCGGGTGTGGGAAG-3'; *PSA* forward 5'-
571 GAGCACCCCTATCAACCCCCTATT -3' , reverse 5'-
572 AGCAACCCTGGACCTCACACCTAA-3'; *ZMYND11,* forward 5'-
573 ATGGCACGTTTAACAAAAAGACG-3', reverse 5'-
574 CGGTCAATGTTGGCAATCTGC-3'; *BRD2*, forward 5'-

575 CTACGTAAGAAACCCCGGAAG-3’, reverse 5’-GCTTTTTCTCCAAAGCCAGTT-
576 3; *TRIM24*, forward 5`-CAGCCACAAATGCCTAAGCAG-3’, reverse 5’-
577 GTGTTGGGAACTTGGATAACTGG-3; *NCOA3*, forward 5’-
578 AGACGGGAGCAGGAAAGTAAA-3’, reverse 5’-
579 GTAAAAGCGGTCCTAAGGAGTC-3’; *DEK*, forward 5’-
580 AACTGCTTTACAACAGGCCAG-3’, reverse 5’-ATGGTTTGCCAGAAGGCTTTG-
581 3’.
582

583 **RNA-Seq of VCaP, LNCaP and LuCaP cells**

584 RNA sequencing for all experiments involving LuCaP xenografts, VCaP and LNCaP
585 cells was performed at the Institute of Oncology Research using Next Ultra II Directional
586 RNA Library Prep Kit for Illumina and sequenced on the Illumina NextSeq500 with single-
587 end, 75 base pair long reads. The overall quality of sequencing reads was evaluated using
588 a variety of tools, namely FastQC (Andrews S., 2010), RSeQC[45], AfterQC[46] and
589 Qualimap[47]. Sequence alignments to the reference human genome (GRCh38) was
590 performed using STAR [48] (v.2.5.2a). Gene-expression was quantified at gene level by using
591 the comprehensive annotations made available by Gencode[49]. Specifically, we used *v27*
592 release of the Gene Transfer File (GTF). Raw-counts were further processed in the *R*
593 Statistical environment and downstream differential expression analysis was performed
594 using the DESeq2[50] pipeline.

595 Genes being expressed at very low levels were automatically filtered out through the
596 *Independent Filtering* feature embedded in DESeq2 (alpha = 0.05). Differential-expression
597 results were ranked according to the computed Wald-statistics values. Subsequently, gene-

598 set enrichment testing was performed using Camera[51] pre-ranked (inter-gene correlation
599 equal to 0.1, parametric test procedure). Statistical enrichments were assessed for gene-sets
600 belonging to the Hallmark collection, which is curated by the Molecular Signature
601 DataBase[52,53] (*MSigDB*), and for custom ERG and DHT-specific gene-signatures. All
602 enrichments were corrected for multiple testing using Benjamini and Hochberg FDR
603 adjusted p-value.
604

605 **Identification of ERG and AR related gene signatures**

606 We retrieved RNA-seq data from GEO Dataset *GSE83652*[14] to identify transcriptional
607 perturbations in VCaP cells following treatment with DHT or following silencing of ERG.
608 To this purpose we completely reprocessed samples SRR3713255-57, SRR3713267-72
609 using *STAR* and *DESeq2* as previously described for VCaP cells. In addition, to identify
610 direct targets, we integrated information relative to AR and ERG chromatin binding sites,
611 which we derived from GEO Dataset *GSE28950*[25]. To maximize the number of peaks and
612 to reduce false negatives, we merged results of experiments performed at different time
613 points, namely 2h and 18h after DHT exposure. De-multiplexed reads were aligned to *hg38*
614 release of the human reference genome using bwa-mem[54] (0.7.15). MACS[55] (v.2.1.0) was
615 used to perform peak calling procedure using a cutoff FDR q-value of 0.01 and a mappable
616 genome size optimized for *hg38* equal to 2.9 gigabases. Downstream analysis was
617 performed in R statistical environment. We identified binding sites overlapping promoters
618 by using bedtools[56].

619 Promoters were defined as DNA regions ranging from 1500 *bp* upstream to 500 *bp*
620 downstream of Transcription Start Sites (TSSs).

621 To discriminate between ERG- and AR- specific transcriptional responses we stratified
622 genes into three main classes: genes whose promoter regions are bound by *AR* but not by
623 *ERG*, genes whose promoters are bound by ERG but not by *AR*, and finally, genes whose
624 promoters are co-bound by both AR and ERG. AR bound only genes were further
625 subdivided into two sets, those being significantly (FDR<0.05) induced following DHT
626 treatment and those being significantly repressed. A similar approach was applied to ERG
627 bound only genes, where genes were subdivided into ERG-induced and ERG-repressed
628 gene-sets, if they were respectively down or up-regulated following *ERG* silencing. To be
629 more stringent in the definition of AR-specific and ERG-specific signatures, we excluded
630 genes from the ERG-induced set that were also significantly up-regulated following DHT
631 treatment, *vice-versa* we excluded ERG-repressed genes that were significantly down-
632 regulated following DHT-treatment. The same criteria were applied for DHT-specific
633 gene-sets. Finally, defined an additional gene-set (DHT-induced/ERG-repressed)
634 consisting of genes being co-bound by AR and ERG in their promoter region, which were
635 significantly up-regulated following DHT treatment but also significantly upregulated
636 following ERG-silencing. All gene-sets are detailed in Supplementary Table 1. Overlap
637 between custom derived gene-signatures and the most represented Hallmark's gene-sets
638 was assessed using GeneOverlap R package (Shen L, Sinai M, 2013). Two-dimensional
639 network visualization was generated with Cytoscape. [57]
640

641 **Gene-set testing and RNA-Seq data processing of clinical samples**

642 Publicly available RNA-Seq data for primary prostate cancer were obtained from The
643 Caner Genome Atlas[3] (TCGA) database and retrieved from Genomics Data Commons

644 (GDC) in form of gene-centric raw counts, using *TCGAbiolinks* package[58]. We selected
645 individuals characterized by either SPOP or ERG fusion, and a third group defined as
646 "others", which includes all remaining samples, excluding those patients exhibiting any
647 other ETS-rearrangement. Differential expression and gene-set enrichment between
648 samples harboring ERG fusions and SPOP-mutations were performed using *DESeq2* and
649 *Camera* (pre-ranked) as previously described for prostate cancer cells. Single-sample gene-
650 set enrichment analysis (GSVA[59] package) was applied to measure, for each individual
651 patient, the overall activity of the custom gene-sets that were previously generated in VCaP
652 cells. Following differential expression analysis between ERG-rearranged and SPOP
653 mutant primary tumors, we defined two gene-sets consisting of SPOP-upregulated (n =
654 443, $\log_2$FC >1, FDR<0.05) and ERG-upregulated (n = 359, $\log_2$FC >1, FDR<0.05) genes.
655 *PolyA+* RNASeq data for metastatic prostate cancer were obtained from SU2C
656 cohort[60]. Normalized *RPKM* values, retrieved through *cBioportal*, were log transformed
657 and patient's categorization (SPOP/ERG/OTHER) was performed in the same manner as
658 for primary tumors. To evaluate whether transcriptional differences occurring between
659 ERG-rearranged and SPOP-mutant individuals were also conserved in CRPC setting, we
660 quantified the above mentioned SPOP-upregulated/ERG-upregulated signatures in the
661 SU2C 2019 cohort, using single-sample gene-set enrichment analysis. The obtained
662 ssGSEA scores were scaled in a range between -1 and 1 (SPOP-Upregulated) and between
663 1 and -1 (ERG-upregulated, inverted). Subsequently we averaged these rescaled values in
664 order to obtain an aggregate score.
665
666 **Circular representation of interactions between gene-sets**

667 Chord diagrams were generated using circlize[61] package in R statistical environment.
668 Strings, whose thickness is proportional to the number of shared elements, represent
669 common genes between sets.
670
671 **ZMYND11 ChIP-seq in VCaP cells**
672 ChIP-seq using anti-ZMYND11 antibody (NBP2-20960, Novus Biologicals) was
673 performed in VCaP cells, overexpressing either wild-type SPOP or mutant SPOP harboring
674 Y87C point mutation. Briefly, to isolate chromatin, cells (120.000.000 per IP) were cross-
675 linked using 1% Formaldehyde cross-link protein-DNA complexes and crosslinking was
676 terminated by the addition of 1/10 volume 1.25 M glycine for 5 min at room temperature
677 followed by cell lysis and sonication, resulting in an average chromatin fragment size of
678 200 bp. Samples lysis was performed as previously described using MNase enzyme 1000
679 gel units=1 uL[62]. After adding the MNase sonication buffer, the samples were sonicated
680 for 30 cycles, 30 sec ON and 30 sec OFF at high voltage. ChIP and input DNA (50 ng)
681 were used for indexed library preparation using NEBNext Ultra II DNA Library Prep kit
682 and subjected to 75 *bp* single-end sequencing on the Illumina NextSeq500. All procedures
683 were performed at the Institute of Oncology Research. De-multiplexed reads were aligned
684 to *hg38* release of the human reference genome using bwa-mem[54] (0.7.15). MACS[55]
685 (v.2.1.0) was used to perform peak calling procedure using a cutoff FDR q-value of 0.01
686 and a mappable genome size optimized for *hg38* equal to 2.9 gigabases. Downstream
687 analysis was performed in R statistical environment. ChIPseeker[63] was used to annotate
688 peaks and to represent the distribution of ZMYND11 binding sites relative to Transcription
689 Start Sites (TSSs). The R package chipenrich[64] was subsequently used to determine

690 enrichment or depletion of ZMYND11 peaks in regions surrounding *TSSs* of genes that are
691 included in Hallmarks or custom gene-set collections. Surrounding regions were defined
692 as ranging from 5kb upstream to 5kb downstream of their *TSSs* (locusdef = 5kb), which is
693 in line with the overall behavior of ZMYND11 binding sites around *TSSs* (Supplementary
694 Fig. 6f-g).
695
696 **Identification of AR-binding sites in primary prostate cancer specimen**
697 Publicly available ChIP-Seq data were retrieved from GSE120738[3]. ChIP-seq data were
698 reprocessed as described for ZMYND11 samples. Differential binding affinity of AR
699 between ERG-rearranged and SPOP-mutant tumors was performed using DiffBind (Stark
700 R and Brown G, 2011).
701
702 **Frequency of SPOP mutations across patients' cohorts**
703 We defined the percentage of SPOP-mutant and TMPRSS2-ERG positive tumors
704 across different patients' cohorts originating from multiple sources. Patients with
705 primary/loco-regional prostate tumors were derived from TCGA and MSK-IMPACT
706 Clinical Sequencing cohorts[34]. Patients with tumor-progression (non-castrate) were
707 derived from MSK-IMPACT and TCGA cohorts, by including from the latter only
708 individuals that showed tumor-progression based on survival information. Castration
709 resistant prostate cancer patients were retrieved from MSK-IMPACT, Beltran et. al[65] and
710 from the SU2C[60] .datasets. Neuroendocrine prostate cancer samples were retrieved from
711 the SU2C cohort (samples annotated with neuroendocrine features) and from Beltran et
712 al[65]. Total number of *SPOP*-mutant and *TMPRSS2-ERG* tumors were determined based

713 on the clinical annotations of the individual studies and integrated with fusion information
714 from TCGA Fusion Gene Database (www.tumorfusions.org). Survival analysis was
715 performed in R statistical environment using the TCGA and MSK-IMPACT clinical
716 sequencing cohort.
717

718 **Quantitative liquid-chromatography-mass spectrometry (LC-MS/MS)**

719 In solution digestion VCaP cell pellets were lysed at 4 ºC in 8 M urea, 50 mM Tris-
720 HCl pH 8.0, 150 mM NaCl, 1 mM EDTA, 2 µg/µl aprotinin (Sigma-Aldrich), 10 µg/µl
721 leupeptin (Roche), and 1 mM phenylmethylsulfonyl fluoride (PMSF) (Sigma). Protein
722 concentration was determined using a bicinchoninic acid (BCA) protein assay (Pierce).
723 Proteins were reduced with 5 mM (DTT) for 45 min at room temperature (RT), followed
724 by alkylation with 10 mM iodoacetamide for 30 min at room temperature in the dark. The
725 urea concentration was reduced to 2 M using 50 mM Tris-HCl, pH 8. Samples were
726 digested for 2 h at 25 ºC with endoproteinase Lys-C (Wako Laboratories) at an enzyme-to-
727 substrate ratio of 1:50. Samples were subsequently digested overnight at 25 ºC with
728 sequencing grade trypsin (Promega) at an enzyme-to-substrate ratio of 1:50. Following
729 overnight digestion, samples were acidified to a final concentration of 1% formic acid.

730 Peptide samples were desalted on a 100 mg tC18 Sep-Pak SPE cartridge (Waters).
731 Cartridges were conditioned with 1 mL of 100% MeCN, 1 mL of 50% MeCN/0.1% FA,
732 and 4x with 1 mL of 0.1% TFA. The sample was loaded, and washed 3x with 1 mL of 0.1%
733 TFA, 1x with 1 mL of 1% FA, and eluted 2x with 600 µl of 50% MeCN/0.1% FA.
734

735 **TMT labeling of peptides**

736 Peptides were labeled with TMT 10-plex isobaric mass tagging reagents (Thermo
737 Fisher Scientific). Each TMT reagent was resuspended in 41 µL of MeCN. Peptides were
738 resuspended in 100 µL of 50 mM HEPES and combined with TMT reagent. Samples were
739 incubated at RT for 1 h while shaking. The TMT reaction was quenched with 8 µL of 5%
740 hydroxylamine at RT for 15 min with shaking. TMT labeled samples were combined, dried
741 to completion, reconstituted in 100 µL of 0.1% FA, and desalted on StageTips or 100 mg
742 SepPak columns as described above.
743

744 **Basic Reverse Phase (bRP) Fractionation**

745 The TMT labeled samples were fractionated using offline high pH reversed-phase
746 chromatography (bRP) as previously described [Mertins et al Nat Prot]. Samples were
747 fractionated using Zorbax 300 Extend C18 column (4.6 × 250 mm, 300 Å, 5 µm, Agilent)
748 on an Agilent 1100 series high-pressure liquid chromatography (HPLC) system. Samples
749 were reconstituted in 900 µL of 4.5 mM ammonium formate (pH 10) in 2% (vol/vol)
750 acetonitrile (MeCN) (bRP solvent A). Samples were injected with Solvent A at a flow rate
751 of 1 mL/min and separated using a 96 min gradient. The gradient consisted of an initial
752 increase to 16% solvent B (90% MeCN, 5 mM ammonium formate, pH 10), followed by
753 60 min linear gradient from 16% solvent B to 40% B and successive ramps to 44% and
754 60% at a flow rate of 1 mL/min. Fractions were collected in a 96-deep well plate (GE
755 Healthcare) and pooled in a non-contiguous manner into final 24 proteome fractions.
756 Pooled fractions were dried to completeness using a SpeedVac concentrator.
757

758 **Liquid chromatography and mass spectrometry**

759 Desalted peptides were resuspended in 3% MeCN/0.1% FA and analyzed by online
760 nanoflow liquid chromatography tandem mass spectrometry (LC-MS/MS) using Q-
761 Exactive plus mass spectrometer (Thermo Fisher Scientific) coupled on-line to a Proxeon
762 Easy-nLC 1200 as previously described [Mertins et al Nature Protocols]. Briefly, 1 ug of
763 each sample was loaded onto a microcapillary column (360 μm outer diameter × 75 μ
764 m inner diameter) containing an integrated electrospray emitter tip (10 μm), packed to
765 approximately 22 cm with ReproSil-Pur C18-AQ 1.9 μm beads (Dr. Maisch GmbH) and
766 heated to 50 ^{o}C. Samples were analyzed with 110 min LC-MS method. The 110 min
767 method contained a mobile phase with a flow rate of 200 nL/min, comprised of 3%
768 acetonitrile/0.1% formic acid (Solvent A) and 90% acetonitrile/0.1% formic acid (Solvent
769 B), with the following gradient profile: (min:%B) 0:2; 1:6; 85:30; 94:60; 95:90; 100:90;
770 101:50; 110:50 (the last two steps at 500 nL/min flow rate). The Q-Exactive plus MS was
771 operated in the data-dependent mode acquiring HCD MS/MS scans (r =35,000) after each
772 MS1 scan (r = 70,000) on the 12 most abundant precursor ions using an MS1 target of 3
773 × 10^6 and an MS2 target of 5 × 10^4 . The maximum ion time utilized for MS/MS
774 scans was 120 ms; the HCD-normalized collision energy was set to 30; the dynamic
775 exclusion time was set to 20 s, isotope exclusion function was enabled, and peptide match
776 function was set to preferred. Charge exclusion was enabled for charge states that were
777 unassigned, 1 and >6.
778

779 **MS Data Analysis**

780 All data were analyzed using Spectrum Mill software package v 6.1 pre-release
781 (Agilent Technologies). Similar MS/MS spectra acquired on the same precursor m/z within

782 +/- 60 s were merged. MS/MS spectra were excluded from searching if they were not
783 within the precursor MH+ range of 750-4000 Da or if they failed the quality filter by not
784 having a sequence tag length >0. MS/MS spectra were searched against UniProt human
785 database. All spectra were allowed +/- 20 ppm mass tolerance for precursor and product
786 ions, 30% minimum matched peak intensity, and "trypsin allow P" enzyme specificity with
787 up to 4 missed cleavages. The fixed modifications were carbamidomethylation at cysteine,
788 and TMT at N-termini and internal lysine residues. Variable modifications included
789 oxidized methionine and N-terminal protein acetylation. Individual spectra were
790 automatically designated as confidently assigned using the Spectrum Mill autovalidation
791 module. Specifically, a target-decoy based false-discovery rate (FDR) scoring threshold
792 criteria via a two-step auto threshold strategy at the spectral and protein levels was used.
793 First, peptide mode was set to allow automatic variable range precursor mass filtering with
794 score thresholds optimized to yield a spectral level FDR of 1 %. A protein polishing
795 autovalidation was applied to further filter the peptide spectrum matches using a target
796 protein-level FDR threshold of 0. Following autovalidation, a protein-protein comparison
797 table was generated, which contained experimental ratios. For all experiments, non-human
798 contaminants and reversed hits were removed. Furthermore, data were filtered to only
799 consider proteins with 2 or more unique peptides and was median normalized.
800

801 **Statistical analysis**

802 GraphPad Prism version 8.3 (GraphPad Software) was used for statistical analysis.
803 Data are depicted as mean + s.e.m. unless otherwise specified. The number of independent
804 experiments or mice used is indicated in each figure legends. Unpaired Student's t-test was

used for comparisons between two groups, one-way analysis of variance (ANOVA) with multiple comparisons for two groups or more, and two-way ANOVA with multiple comparisons for repeated measurements. Multiple comparisons tests were corrected by controlling the False Discovery Rate (FDR) using Benjamini and Hochberg's method. . Correlation analyses were performed using Pearson correlation coefficients.

Data Availability

The original mass spectra have been deposited in the public proteomics repository MassIVE and are accessible at ftp://MSV000082915@massive.ucsd.edu when providing the dataset password: prostate. If requested, also provide the username: MSV000082915. This data will be made public upon acceptance of the manuscript.

RNA-Seq data generated have been deposited in the *ArrayExpress* database at EMBL-EBI and were assigned the accessions *E-MTAB-7165, E-MTAB-7170, E-MTAB-7173*. These data are accessible when providing the datasets username and password as follow:

Username: *Reviewer_E-MTAB-7165* Password: *4sJqpicv*

Username: *Reviewer_E-MTAB-7170* Password: *AAA65MMy*

Username: *Reviewer_E-MTAB-7173* Password*: sIpcob0o*.

CHiP-Seq data generated have been deposited in the *ArrayExpress* database at EMBL-EBI and were assigned the accessions *E-MTAB-7174*. These data are accessible when providing the dataset username and password as follow:

Username: *Reviewer_E-MTAB-7174* Password: *onwwwwni*

All these data will be made public upon acceptance of the manuscript.

References

1 Mina, M. *et al.* Conditional Selection of Genomic Alterations Dictates Cancer Evolution and Oncogenic Dependencies. *Cancer cell* **32**, 155-168.e156, doi:10.1016/j.ccell.2017.06.010 (2017).

2 Davies, H. *et al.* Mutations of the BRAF gene in human cancer. *Nature* **417**, 949-954, doi:10.1038/nature00766 (2002).

3 TCGA. The Molecular Taxonomy of Primary Prostate Cancer. *Cell* **163**, 1011-1025, doi:10.1016/j.cell.2015.10.025 (2015).

4 Barbieri, C. E. *et al.* Exome sequencing identifies recurrent SPOP, FOXA1 and MED12 mutations in prostate cancer. *Nature genetics* **44**, 685-689, doi:10.1038/ng.2279 (2012).

5 Baca, S. C. *et al.* Punctuated evolution of prostate cancer genomes. *Cell* **153**, 666-677, doi:10.1016/j.cell.2013.03.021 (2013).

6 Robinson, D. *et al.* Integrative clinical genomics of advanced prostate cancer. *Cell* **161**, 1215-1228, doi:10.1016/j.cell.2015.05.001 (2015).

7 Grasso, C. S. *et al.* The mutational landscape of lethal castration-resistant prostate cancer. *Nature* **487**, 239-243, doi:10.1038/nature11125 (2012).

8 Gan, W. *et al.* SPOP Promotes Ubiquitination and Degradation of the ERG Oncoprotein to Suppress Prostate Cancer Progression. *Molecular cell* **59**, 917-930, doi:10.1016/j.molcel.2015.07.026 (2015).

9 An, J. *et al.* Truncated ERG Oncoproteins from TMPRSS2-ERG Fusions Are Resistant to SPOP-Mediated Proteasome Degradation. *Molecular cell* **59**, 904-916, doi:10.1016/j.molcel.2015.07.025 (2015).

10 Shoag, J. *et al.* SPOP mutation drives prostate neoplasia without stabilizing oncogenic transcription factor ERG. *The Journal of clinical investigation*, doi:10.1172/JCI96551 (2017).

11 Blattner, M. *et al.* SPOP Mutation Drives Prostate Tumorigenesis In Vivo through Coordinate Regulation of PI3K/mTOR and AR Signaling. *Cancer cell* **31**, 436-451, doi:10.1016/j.ccell.2017.02.004 (2017).

12 King, J. C. *et al.* Cooperativity of TMPRSS2-ERG with PI3-kinase pathway activation in prostate oncogenesis. *Nature genetics* **41**, 524-526, doi:10.1038/ng.371 (2009).

13 Carver, B. S. *et al.* Aberrant ERG expression cooperates with loss of PTEN to promote cancer progression in the prostate. *Nature genetics* **41**, 619-624, doi:10.1038/ng.370 (2009).

14 Bose, R. *et al.* ERF mutations reveal a balance of ETS factors controlling prostate oncogenesis. *Nature* **546**, 671-675, doi:10.1038/nature22820 (2017).

15 Saar, M. *et al.* Spheroid culture of LuCaP 147 as an authentic preclinical model of prostate cancer subtype with SPOP mutation and hypermutator phenotype. *Cancer letters* **351**, 272-280, doi:10.1016/j.canlet.2014.06.014 (2014).

16 Guo, Z. Q. *et al.* Small-Molecule Targeting of E3 Ligase Adaptor SPOP in Kidney Cancer. *Cancer cell* **30**, 474-484, doi:10.1016/j.ccell.2016.08.003 (2016).

17 Geng, C. *et al.* Androgen receptor is the key transcriptional mediator of the tumor suppressor SPOP in prostate cancer. *Cancer research* **74**, 5631-5643, doi:10.1158/0008-5472.Can-14-0476 (2014).

875 18 Geng, C. *et al.* Prostate cancer-associated mutations in speckle-type POZ
876 protein (SPOP) regulate steroid receptor coactivator 3 protein turnover.
877 *Proceedings of the National Academy of Sciences of the United States of America*
878 **110**, 6997-7002, doi:10.1073/pnas.1304502110 (2013).
879 19 An, J., Wang, C., Deng, Y., Yu, L. & Huang, H. Destruction of full-length androgen
880 receptor by wild-type SPOP, but not prostate-cancer-associated mutants. *Cell*
881 *reports* **6**, 657-669, doi:10.1016/j.celrep.2014.01.013 (2014).
882 20 Theurillat, J. P. *et al.* Prostate cancer. Ubiquitylome analysis identifies
883 dysregulation of effector substrates in SPOP-mutant prostate cancer. *Science*
884 *(New York, N.Y.)* **346**, 85-89, doi:10.1126/science.1250255 (2014).
885 21 Groner, A. C. *et al.* TRIM24 Is an Oncogenic Transcriptional Activator in
886 Prostate Cancer. *Cancer cell*, doi:10.1016/j.ccell.2016.04.012 (2016).
887 22 Zhang, P. *et al.* Intrinsic BET inhibitor resistance in SPOP-mutated prostate
888 cancer is mediated by BET protein stabilization and AKT-mTORC1 activation.
889 *Nature medicine* **23**, 1055-1062, doi:10.1038/nm.4379 (2017).
890 23 Janouskova, H. *et al.* Opposing effects of cancer-type-specific SPOP mutants on
891 BET protein degradation and sensitivity to BET inhibitors. *Nature medicine* **23**,
892 1046-1054, doi:10.1038/nm.4372 (2017).
893 24 Dai, X. *et al.* Prostate cancer-associated SPOP mutations confer resistance to
894 BET inhibitors through stabilization of BRD4. *Nature medicine* **23**, 1063-1071,
895 doi:10.1038/nm.4378 (2017).
896 25 Chng, K. R. *et al.* A transcriptional repressor co-regulatory network governing
897 androgen response in prostate cancers. *The EMBO journal* **31**, 2810-2823,
898 doi:10.1038/emboj.2012.112 (2012).
899 26 Hernandez-Segura, A. *et al.* Unmasking Transcriptional Heterogeneity in
900 Senescent Cells. *Curr Biol* **27**, 2652-2660.e2654,
901 doi:10.1016/j.cub.2017.07.033 (2017).
902 27 Purcell, M., Kruger, A. & Tainsky, M. A. Gene expression profiling of replicative
903 and induced senescence. *Cell cycle (Georgetown, Tex.)* **13**, 3927-3937,
904 doi:10.4161/15384101.2014.973327 (2014).
905 28 Wen, H. *et al.* ZMYND11 links histone H3.3K36me3 to transcription elongation
906 and tumour suppression. *Nature* **508**, 263-268, doi:10.1038/nature13045
907 (2014).
908 29 Mani, R. S. *et al.* TMPRSS2-ERG-mediated feed-forward regulation of wild-type
909 ERG in human prostate cancers. *Cancer research* **71**, 5387-5392,
910 doi:10.1158/0008-5472.CAN-11-0876 (2011).
911 30 Chen, Y. *et al.* ETS factors reprogram the androgen receptor cistrome and
912 prime prostate tumorigenesis in response to PTEN loss. *Nature medicine* **19**,
913 1023-1029, doi:10.1038/nm.3216 (2013).
914 31 Yu, J. *et al.* An integrated network of androgen receptor, polycomb, and
915 TMPRSS2-ERG gene fusions in prostate cancer progression. *Cancer cell* **17**,
916 443-454, doi:10.1016/j.ccr.2010.03.018 (2010).
917 32 Mounir, Z. *et al.* ERG signaling in prostate cancer is driven through PRMT5-
918 dependent methylation of the Androgen Receptor. *eLife* **5**,
919 doi:10.7554/eLife.13964 (2016).

33 Boysen, G. *et al.* SPOP-Mutated/CHD1-Deleted Lethal Prostate Cancer and Abiraterone Sensitivity. *Clinical cancer research : an official journal of the American Association for Cancer Research*, doi:10.1158/1078-0432.ccr-18-0937 (2018).

34 Abida, W. *et al.* Prospective Genomic Profiling of Prostate Cancer Across Disease States Reveals Germline and Somatic Alterations That May Affect Clinical Decision Making. *JCO Precis Oncol* **2017**, doi:10.1200/PO.17.00029 (2017).

35 Teply, B. A. *et al.* Bipolar androgen therapy in men with metastatic castration-resistant prostate cancer after progression on enzalutamide: an open-label, phase 2, multicohort study. *The Lancet. Oncology* **19**, 76-86, doi:10.1016/S1470-2045(17)30906-3 (2018).

36 Zhao, D. *et al.* Synthetic essentiality of chromatin remodelling factor CHD1 in PTEN-deficient cancer. *Nature* **542**, 484-488, doi:10.1038/nature21357 (2017).

37 Lee, S. C. *et al.* Synthetic Lethal and Convergent Biological Effects of Cancer-Associated Spliceosomal Gene Mutations. *Cancer cell* **34**, 225-241.e228, doi:10.1016/j.ccell.2018.07.003 (2018).

38 Zeineldin, M. *et al.* MYCN amplification and ATRX mutations are incompatible in neuroblastoma. *Nat Commun* **11**, 913, doi:10.1038/s41467-020-14682-6 (2020).

39 Cole, C. B. *et al.* PML-RARA requires DNA methyltransferase 3A to initiate acute promyelocytic leukemia. *The Journal of clinical investigation* **126**, 85-98, doi:10.1172/jci82897 (2016).

40 Ley, T. J. *et al.* Genomic and epigenomic landscapes of adult de novo acute myeloid leukemia. *The New England journal of medicine* **368**, 2059-2074, doi:10.1056/NEJMoa1301689 (2013).

41 Beshiri, M. L. *et al.* A PDX/Organoid Biobank of Advanced Prostate Cancers Captures Genomic and Phenotypic Heterogeneity for Disease Modeling and Therapeutic Screening. *Clin Cancer Res* **24**, 4332-4345, doi:10.1158/1078-0432.CCR-18-0409 (2018).

42 Tomlins, S. A. *et al.* Distinct classes of chromosomal rearrangements create oncogenic ETS gene fusions in prostate cancer. *Nature* **448**, 595-599, doi:10.1038/nature06024 (2007).

43 Drost, J. *et al.* Organoid culture systems for prostate epithelial and cancer tissue. *Nature protocols* **11**, 347-358, doi:10.1038/nprot.2016.006 (2016).

44 Corey, E. *et al.* LuCaP 35: a new model of prostate cancer progression to androgen independence. *Prostate* **55**, 239-246, doi:10.1002/pros.10198 (2003).

45 Wang, L., Wang, S. & Li, W. RSeQC: quality control of RNA-seq experiments. *Bioinformatics (Oxford, England)* **28**, 2184-2185, doi:10.1093/bioinformatics/bts356 (2012).

46 Chen, S. *et al.* AfterQC: automatic filtering, trimming, error removing and quality control for fastq data. *BMC Bioinformatics* **18**, 80, doi:10.1186/s12859-017-1469-3 (2017).

965 47 Garcia-Alcalde, F. *et al.* Qualimap: evaluating next-generation sequencing
966 alignment data. *Bioinformatics (Oxford, England)* **28**, 2678-2679,
967 doi:10.1093/bioinformatics/bts503 (2012).
968 48 Dobin, A. *et al.* STAR: ultrafast universal RNA-seq aligner. *Bioinformatics*
969 *(Oxford, England)* **29**, 15-21, doi:10.1093/bioinformatics/bts635 (2013).
970 49 Harrow, J. *et al.* GENCODE: the reference human genome annotation for The
971 ENCODE Project. *Genome research* **22**, 1760-1774,
972 doi:10.1101/gr.135350.111 (2012).
973 50 Love, M. I., Huber, W. & Anders, S. Moderated estimation of fold change and
974 dispersion for RNA-seq data with DESeq2. *Genome biology* **15**, 550,
975 doi:10.1186/s13059-014-0550-8 (2014).
976 51 Wu, D. & Smyth, G. K. Camera: a competitive gene set test accounting for inter-
977 gene correlation. *Nucleic acids research* **40**, e133, doi:10.1093/nar/gks461
978 (2012).
979 52 Liberzon, A. *et al.* The Molecular Signatures Database (MSigDB) hallmark gene
980 set collection. *Cell Syst* **1**, 417-425, doi:10.1016/j.cels.2015.12.004 (2015).
981 53 Liberzon, A. *et al.* Molecular signatures database (MSigDB) 3.0. *Bioinformatics*
982 *(Oxford, England)* **27**, 1739-1740, doi:10.1093/bioinformatics/btr260 (2011).
983 54 Li, H. & Durbin, R. Fast and accurate long-read alignment with Burrows-
984 Wheeler transform. *Bioinformatics (Oxford, England)* **26**, 589-595,
985 doi:10.1093/bioinformatics/btp698 (2010).
986 55 Zhang, Y. *et al.* Model-based analysis of ChIP-Seq (MACS). *Genome biology* **9**,
987 R137, doi:10.1186/gb-2008-9-9-r137 (2008).
988 56 Quinlan, A. R. & Hall, I. M. BEDTools: a flexible suite of utilities for comparing
989 genomic features. *Bioinformatics (Oxford, England)* **26**, 841-842,
990 doi:10.1093/bioinformatics/btq033 (2010).
991 57 Shannon, P. *et al.* Cytoscape: a software environment for integrated models of
992 biomolecular interaction networks. *Genome research* **13**, 2498-2504,
993 doi:10.1101/gr.1239303 (2003).
994 58 Colaprico, A. *et al.* TCGAbiolinks: an R/Bioconductor package for integrative
995 analysis of TCGA data. *Nucleic acids research* **44**, e71,
996 doi:10.1093/nar/gkv1507 (2016).
997 59 Hanzelmann, S., Castelo, R. & Guinney, J. GSVA: gene set variation analysis for
998 microarray and RNA-seq data. *BMC Bioinformatics* **14**, 7, doi:10.1186/1471-
999 2105-14-7 (2013).
1000 60 Abida, W. *et al.* Genomic correlates of clinical outcome in advanced prostate
1001 cancer. *Proceedings of the National Academy of Sciences of the United States of*
1002 *America* **116**, 11428-11436, doi:10.1073/pnas.1902651116 (2019).
1003 61 Gu, Z., Gu, L., Eils, R., Schlesner, M. & Brors, B. circlize Implements and enhances
1004 circular visualization in R. *Bioinformatics (Oxford, England)* **30**, 2811-2812,
1005 doi:10.1093/bioinformatics/btu393 (2014).
1006 62 Yokoyama, Y. *et al.* BET Inhibitors Suppress ALDH Activity by Targeting
1007 ALDH1A1 Super-Enhancer in Ovarian Cancer. *Cancer Res* **76**, 6320-6330,
1008 doi:10.1158/0008-5472.can-16-0854 (2016).

1009 63 Yu, G., Wang, L. G. & He, Q. Y. ChIPseeker: an R/Bioconductor package for ChIP
1010 peak annotation, comparison and visualization. *Bioinformatics (Oxford,*
1011 *England)* **31**, 2382-2383, doi:10.1093/bioinformatics/btv145 (2015).
1012 64 Welch, R. P. *et al.* ChIP-Enrich: gene set enrichment testing for ChIP-seq data.
1013 *Nucleic acids research* **42**, e105, doi:10.1093/nar/gku463 (2014).
1014 65 Beltran, H. *et al.* Divergent clonal evolution of castration-resistant
1015 neuroendocrine prostate cancer. *Nature medicine* **22**, 298-305,
1016 doi:10.1038/nm.4045 (2016).
1017

Figure 1

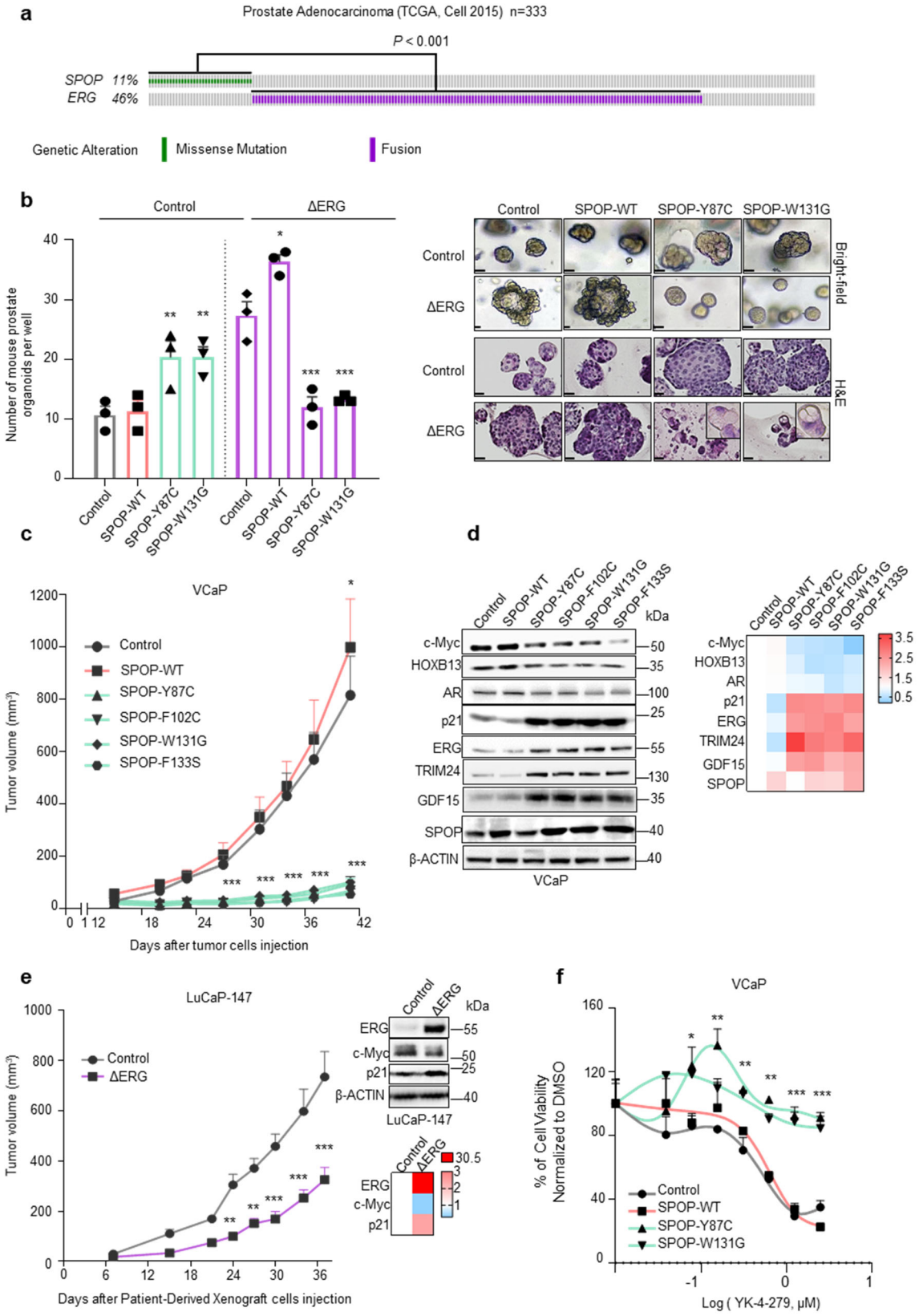
a
Prostate Adenocarcinoma (TCGA, Cell 2015) n=333
P < 0.001
SPOP 11%
ERG 46%
Genetic Alteration
Missense Mutation
Fusion
b
Control
ΔERG
Number of mouse prostate organoids per well
Control
SPOP-WT
SPOP-Y87C
SPOP-W131G
Bright-field
H&E
c
VCaP
Tumor volume (mm³)
Control
SPOP-WT
SPOP-Y87C
SPOP-F102C
SPOP-W131G
SPOP-F133S
Days after tumor cells injection
d
kDa
c-Myc
HOXB13
AR
p21
ERG
TRIM24
GDF15
SPOP
β-ACTIN
VCaP
e
LuCaP-147
Tumor volume (mm³)
Control
ΔERG
Days after Patient-Derived Xenograft cells injection
f
VCaP
% of Cell Viability Normalized to DMSO
Log (YK-4-279, μM)

Fig 1. Genetic alterations in *SPOP* and *ERG* are synthetic sick. a Distribution of genetic alterations in *SPOP* and *ERG* across 333 primary prostate cancers in TCGA database[1]. **b** 3D growth of mouse prostate epithelial organoids derived from C57BL/6 mice over-expressing the indicated SPOP and ERG species (bar represents 20 μm) (n=3, technical replicates). Representative bright field pictures and haematoxylin and eosin (H&E) stained sections are shown. **c** *In vivo* growth of VCaP xenografts over-expressing the indicated SPOP species in immune-compromised mice (each group, n=10). **d** Immunoblot of VCaP cells over-expressing the indicated SPOP species and corresponding quantification of the indicated protein levels depicted as heatmap. Protein expression changes were normalized to β-ACTIN and Control cell line. **e** Tumor growth kinetics of xenografts established from LuCaP-147 PDX (SPOP-Y83C) stably overexpressing ΔERG or Control vector (each group, n=10). Corresponding immunoblot and quantification depicted as heatmap. Protein expression changes were normalized to Vinculin (VCL) and Control cell line. **f** Dose-response curve of VCaP cells overexpressing the indicated SPOP species and treated with the ETS-inhibitor YK-4-279. All error bars, mean + s.e.m. P values were determined by one-way ANOVA (b) or two-way ANOVA (c,e,f) with multiple comparisons and adjusted using Benjamini-Hochberg post-test $*P < 0.05$, $**P < 0.01$, $***P < 0.001$. Molecular weights are indicated in kilodaltons (kDa).

Figure 2

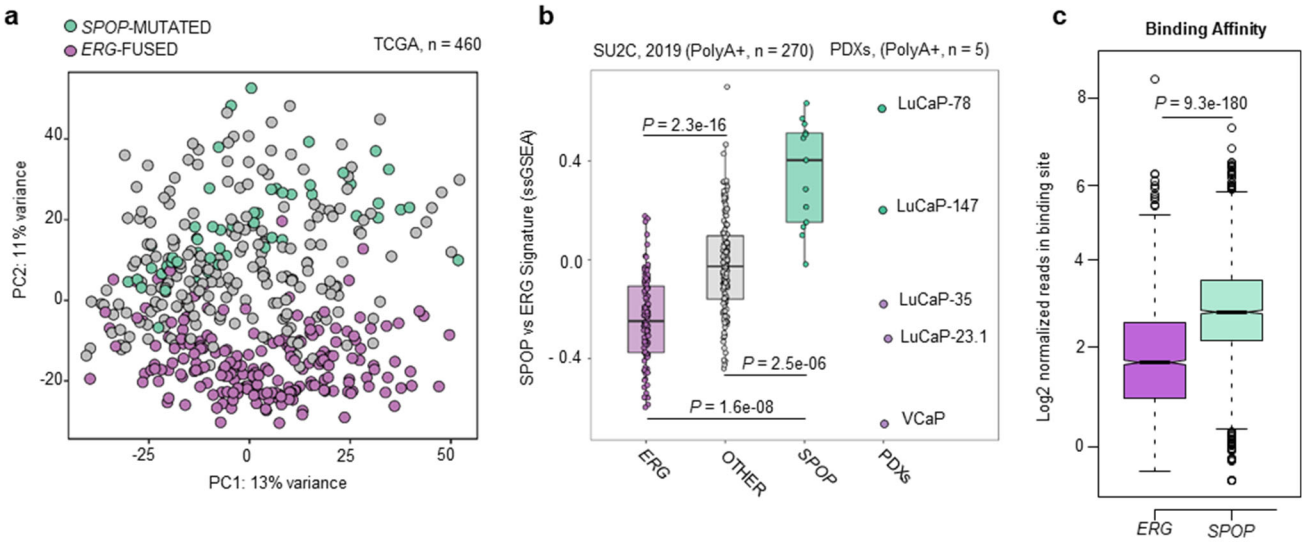

Fig. 2 Transcriptome analysis of primary prostate cancer patients reveals major differences between *SPOP* mutant and *ERG*-fused tumor subtypes. a PCA-analysis based on RNA-Seq derived mRNA expression levels (TCGA cohort). *ERG*-fused (violet) and *SPOP*-mutant (green). Individuals were annotated into subtypes as described in Material and Methods. **b** Boxplots representing the transcriptional activity of SPOP integrated-signature (see Materials and Methods) applied to CRPC samples (SU2C-2019 cohort, left) and PDX-models. Scores are determined genes-signatures derived from primary prostate tumors (TCGA-cohort). ERG-fused samples are depicted in violet, SPOP-mutant samples are depicted in green. Samples not harboring SPOP mutations or ERG rearrangements are represented in grey. *P*-values were determined using Wilcoxon-test. **c** Boxplots depicting the amount of normalized reads per binding site across all the differentially bound (DB) regions (FDR = 0.05) resulting from the comparison between *ERG*-fused (violet) and *SPOP*-mutant (green) samples.

Figure 3

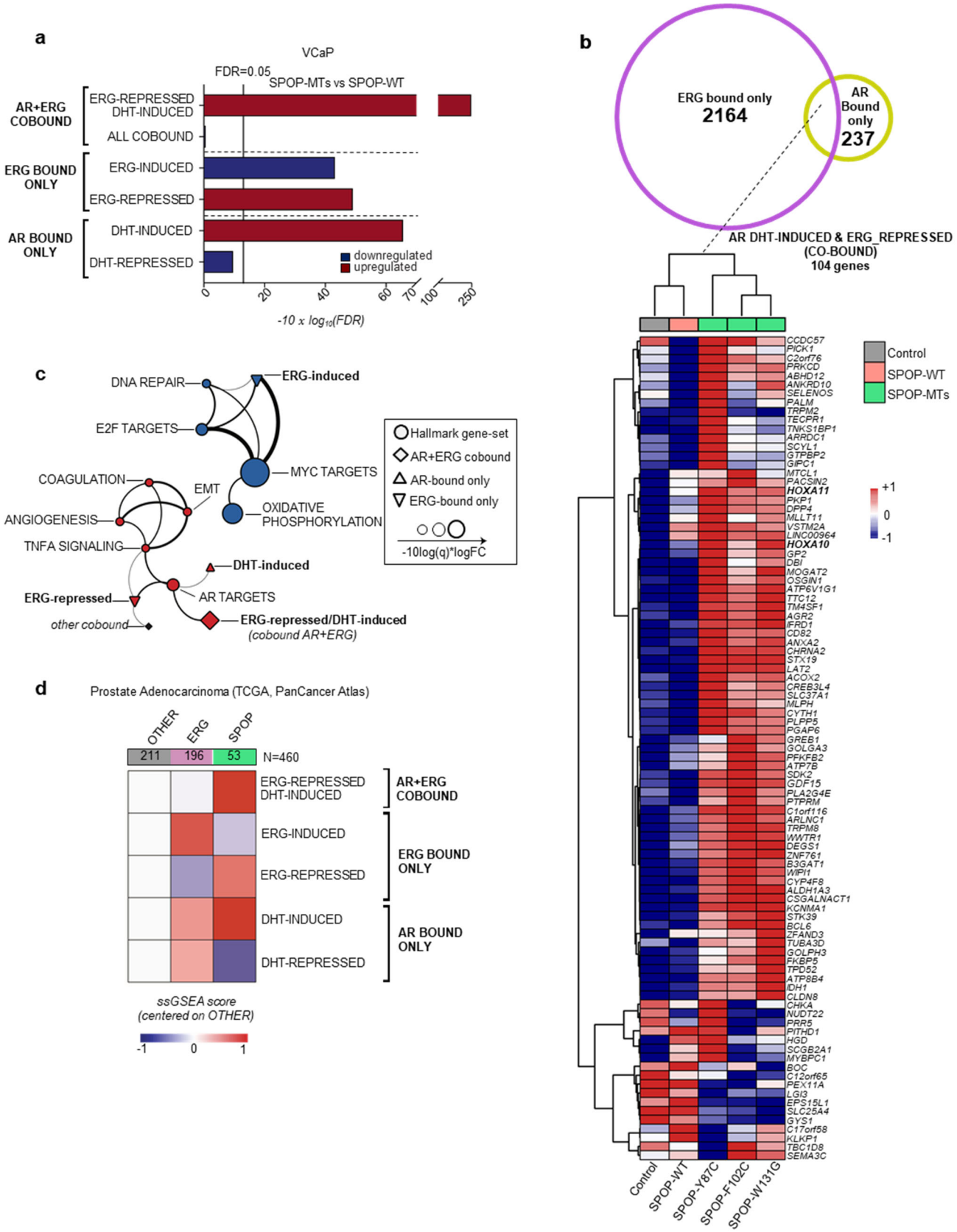
a
VCaP
FDR=0.05
SPOP-MTs vs SPOP-WT
AR+ERG COBOUND
ERG-REPRESSED DHT-INDUCED
ALL COBOUND
ERG BOUND ONLY
ERG-INDUCED
ERG-REPRESSED
AR BOUND ONLY
DHT-INDUCED
DHT-REPRESSED
downregulated
upregulated
0 20 40 60 70 100 250
-10 x log10(FDR)
b
ERG bound only
2164
AR Bound only
237
AR DHT-INDUCED & ERG_REPRESSED (CO-BOUND)
104 genes
Control
SPOP-WT
SPOP-MTs
+1
0
-1
Control
SPOP-WT
SPOP-Y87C
SPOP-F102C
SPOP-W131G
c
DNA REPAIR
ERG-induced
E2F TARGETS
MYC TARGETS
COAGULATION
EMT
ANGIOGENESIS
OXIDATIVE PHOSPHORYLATION
TNFA SIGNALING
DHT-induced
AR TARGETS
ERG-repressed
other cobound
ERG-repressed/DHT-induced
(cobound AR+ERG)
Hallmark gene-set
AR+ERG cobound
AR-bound only
ERG-bound only
-10log(q)*logFC
d
Prostate Adenocarcinoma (TCGA, PanCancer Atlas)
OTHER
ERG
SPOP
211
196
53
N=460
ERG-REPRESSED DHT-INDUCED
AR+ERG COBOUND
ERG-INDUCED
ERG-REPRESSED
ERG BOUND ONLY
DHT-INDUCED
DHT-REPRESSED
AR BOUND ONLY
ssGSEA score
(centered on OTHER)
-1
0
1

Fig. 3 Mutant SPOP-induced androgen receptor signaling antagonizes ERG activity. **a** Gene-set enrichment analysis of VCaP cells overexpressing SPOP mutant (SPOP-MTs; SPOP-Y87C, -F102C, -W131G) versus SPOP-wild type (-WT), based on RNA-seq data. Experiments were performed using three replicates for each condition. Enrichments are determined on custom gene-sets of direct androgen receptor (AR) and ERG target genes (Supplemental Table 1). Enrichments and FDR-adjusted p-values are computed with *Camera* (pre-ranked) **b** Venn Diagram and heatmap depicting the expression of genes included in the custom gene-set of AR/ERG co-bound genes that are repressed by ERG and induced by DHT in VCaP cells overexpressing SPOP-MTs (SPOP-Y87C, F102C, W131G), SPOP-WT and vector Control. Genes (rows) and samples (columns) were clustered using Euclidean distance. Gene expression values were normalized using variance stabilizing transformation (vst) and subsequently scaled and centered by row prior of clustering. Columns represent average expression of three replicates for each condition. **c,** Two-dimensional network representing overlaps between the 10 most significantly enriched Hallmark and custom gene-sets, identified when comparing SPOP-MTs (SPOP-Y87C, F102C, W131G) to SPOP-wild type (-WT) overexpressing VCaP cells. Thickness of edges is proportional to the significance of the overlap of the connected nodes measured by Fisher test. Only edges with FDR value <0.05 are shown. Size of nodes is proportional to gene-set enrichment significance and equals to -10 x $\log_{10}$ (FDR). **d**, Heatmap representing gene-set activity stratified according to tumor subtype, derived from TCGA cohort. For each tumor group, the average value of single sample GSEA scores was considered. Values were scaled and referenced to samples that did not harbor any ETS-fusion (*ERG*, *ETV1*, and *ETV4)* or point mutations in *SPOP*[1].

Figure 4

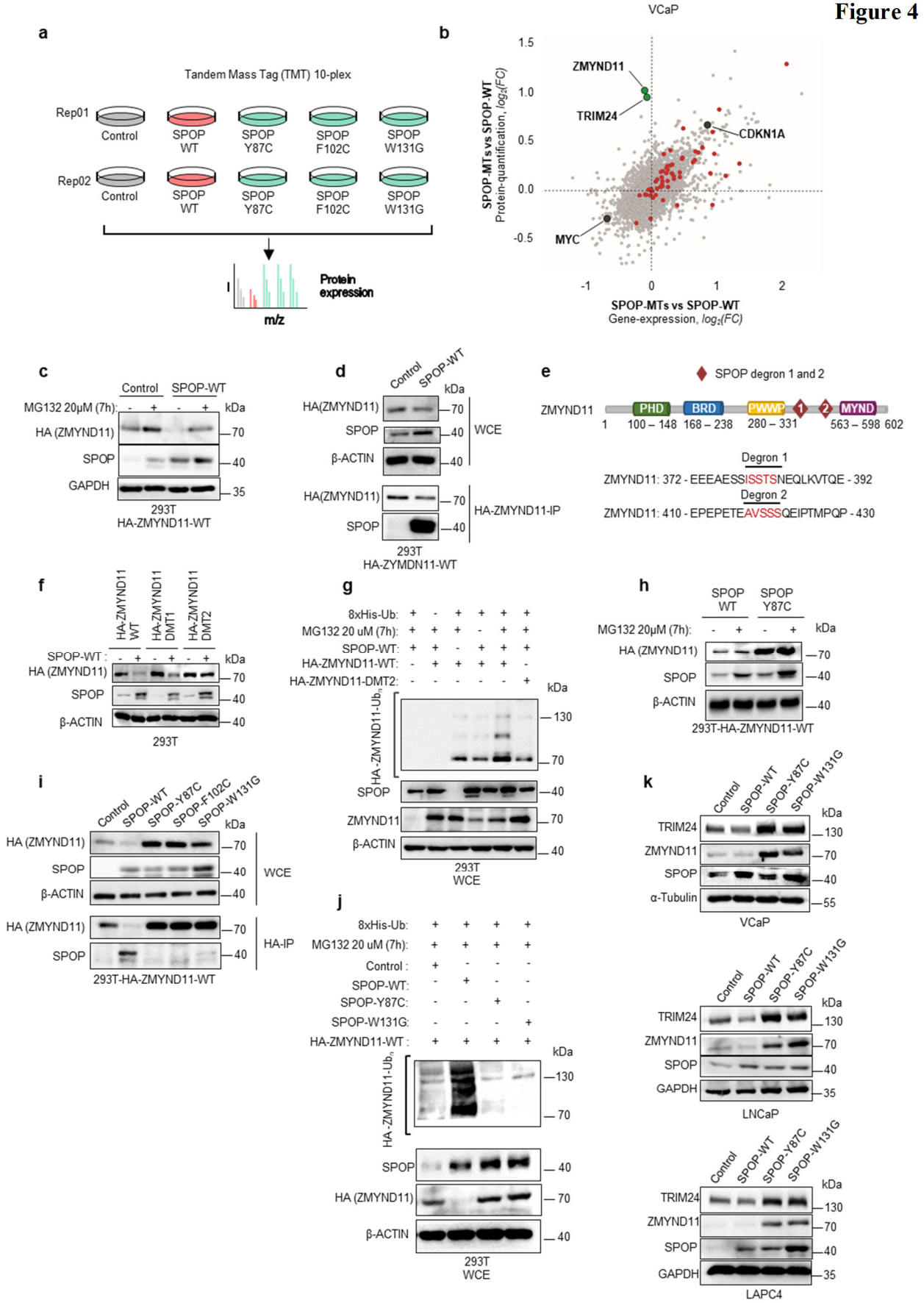
a
Tandem Mass Tag (TMT) 10-plex
Rep01
Control
SPOP WT
SPOP Y87C
SPOP F102C
SPOP W131G
Rep02
Protein expression
m/z
b
VCaP
ZMYND11
TRIM24
CDKN1A
MYC
SPOP-MTs vs SPOP-WT
Protein-quantification, log2(FC)
Gene-expression, log2(FC)
c
Control
SPOP-WT
MG132 20μM (7h):
HA (ZMYND11)
SPOP
GAPDH
293T
HA-ZMYND11-WT
d
HA(ZMYND11)
SPOP
β-ACTIN
WCE
HA-ZMYND11-IP
293T
HA-ZYMDN11-WT
e
SPOP degron 1 and 2
ZMYND11
PHD
BRD
PWWP
MYND
Degron 1
ZMYND11: 372 - EEEAESSISSTSNEQLKVTQE - 392
Degron 2
ZMYND11: 410 - EPEPETEAVSSSQEIPTMPQP - 430
f
HA-ZMYND11 WT
HA-ZMYND11 DMT1
HA-ZMYND11 DMT2
SPOP-WT
293T
g
8xHis-Ub:
MG132 20 uM (7h):
SPOP-WT:
HA-ZMYND11-WT:
HA-ZMYND11-DMT2:
HA-ZMYND11-Ubn
293T
WCE
h
SPOP WT
SPOP Y87C
293T-HA-ZMYND11-WT
i
Control
SPOP-WT
SPOP-Y87C
SPOP-F102C
SPOP-W131G
293T-HA-ZMYND11-WT
j
Control :
SPOP-Y87C:
SPOP-W131G:
HA-ZMYND11-WT :
293T
WCE
k
TRIM24
α-Tubulin
VCaP
LNCaP
LAPC4

Fig. 4 ZMYND11 is a *de novo* SPOP substrate. a Schematic illustration showing the design of the proteomics experiments. Tandem Mass Tag (TMT)-based quantitative mass-spectrometry (n=2, biological replicates) was used in VCaP cells overexpressing Control vector (Control), SPOP-WT, or three different SPOP mutants (SPOP-Y87C, SPOP-F102C and SPOP-W131G). **b** Scatter plot comparing transcriptomic and proteomic derived fold changes resulting from the comparison between SPOP-MTs (average across SPOP-Y87C, -F102C, -W131G) and SPOP-WT VCaP cells. (n=3 biological replicates for transcriptome, n=2 biological replicates for proteome). Genes belonging the DHT-Induced/ERG-Repressed gene-signature (AR+ERG co-bound) are highlighted in red. TRIM24 and ZMYND11 are the most upregulated proteins without changes at mRNA levels and are highlighted in green. CDKN1A (p21) upregulated at both mRNA and protein levels, and MYC downregulated at both mRNA and protein levels, are highlighted in black. **c** Over-expression of HA-ZMYND11 and SPOP-WT in 293T cells and subsequent expression analysis of the indicated proteins by immunoblotting. **d** Whole cell extracts (WCE) of 293T cells over-expressing HA-ZMYND11-WT and different SPOP species and corresponding anti-HA-immunoprecipitation (HA-IP). Expression of the indicated proteins was analyzed by immunoblotting. **e** Domain structure of ZMYND11 with indicated SPOP-degron and ubiquitin sites. **f** Forced expression of SPOP-WT together with HA-ZMYND11-WT or two degron deficient mutants (DMT1 & DMT2) in 293T cells. **g** *In vivo* ubiquitylation assay of HA-ZMYND11 in 293T cells. Cell were transiently transfected with the indicated constructs and histidine-tagged (his-tag), ubiquitylated proteins were pulled down using nickel beads. Ubiquitylated HA-tagged ZMYND11 was detected by immunoblotting. **h** Over-expression of HA-ZMYND11 and SPOP-Y87C in 293T cells and subsequent expression analysis of the indicated proteins by immunoblotting after proteasomal inhibition with MG132. **i** Whole cell extracts (WCE) and corresponding anti-HA-immunoprecipitation (HA-IP) of 293T cells over-expressing HA-ZMYND11-WT and different SPOP-MTs species as indicated. Expression of the indicated proteins was analyzed by immunoblotting. **j** *In vivo* ubiquitylation assay of HA-ZMYND11 in 293T cells. Cell were transiently transfected with the indicated constructs and histidine-tagged (his-tag), ubiquitylated proteins were pulled down using nickel beads. Ubiquitylated HA-tagged ZMYND11 was detected by immunoblotting. **k** Immunoblots of indicated proteins in VCaP, LNCaP and LAPC4 human prostate cancer cells overexpressing the indicated SPOP species. Molecular weights are indicated in kilodaltons (kDa).

Figure 5

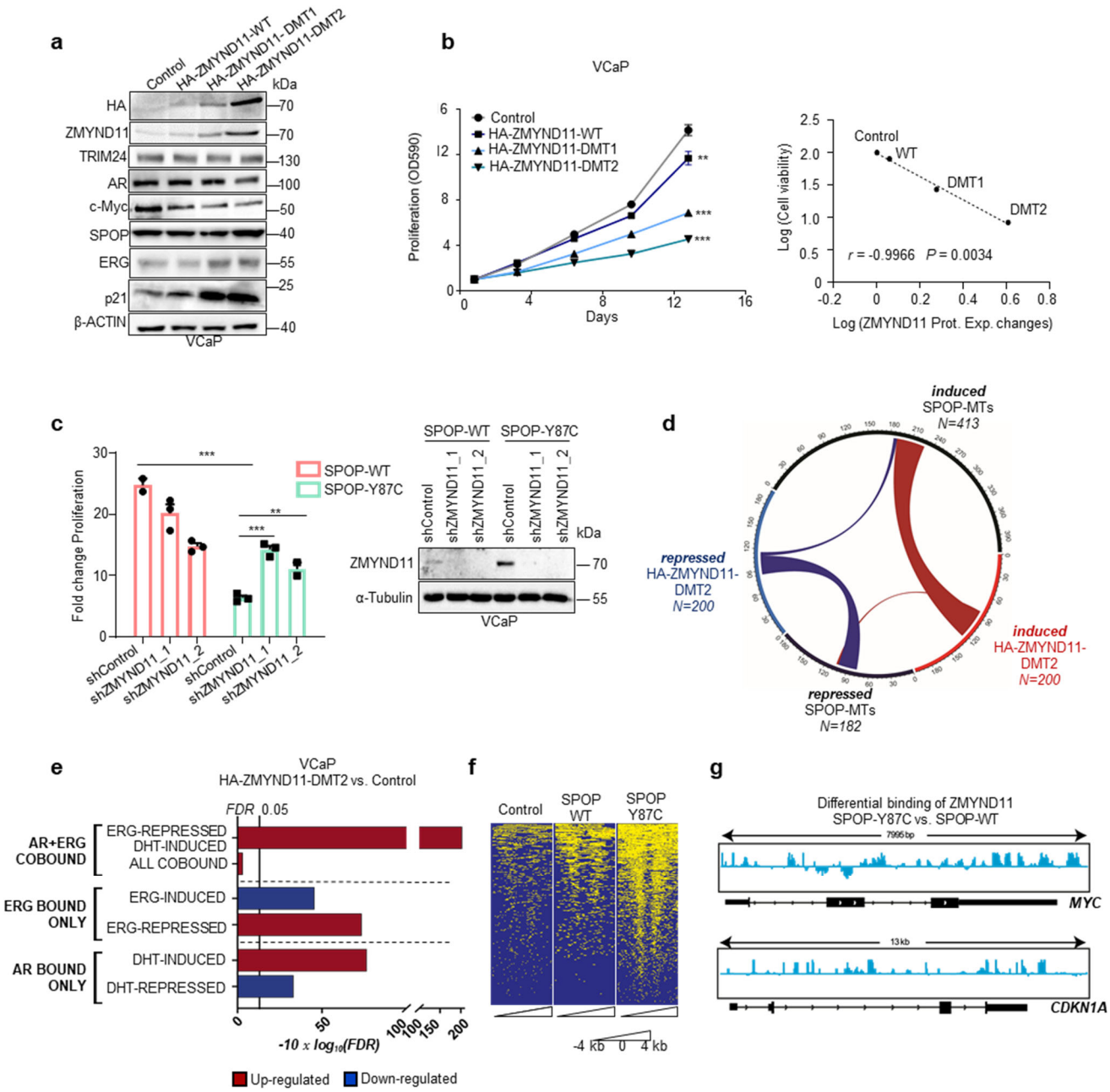

Fig. 5 ZMYND11 induces AR signaling pathway and represses ERG activity. a,b Immunoblot of indicated proteins (**a**) and corresponding 2D proliferation assay (b) of VCaP cancer cells overexpressing HA-ZMNYD11-WT and derived degron-deficient mutants (DMT1/2) (n=3). Correlation between cell viability and ZMYND11 protein expression changes (Prot. Exp. Changes), as quantified by immunoblot in the same cell lines. *P* values were calculated using Pearson rank correlation. **c** Fold-change cell viability of VCaP cancer cells over-expressing the indicated SPOP species with and without

ZMYND11 knockdown using two different short hairpin RNAs, at day 16 (n=3). Protein expression of the indicated proteins was analyzed by immunoblotting. **d** Chord-diagram of transcriptionally regulated genes by either SPOP-MTs or HA-ZMYND11-DMT2 in VCaP cells (FDR<0.05). Strings, whose thickness is proportional to the number of shared elements, represent common genes between sets. **e** Gene-set enrichment analysis of VCaP cell overexpressing HA-ZMYND11-DMT2 compared to Control, based on RNA-seq data. Enrichments are performed on custom gene-sets of direct androgen receptor (AR) and ERG target genes. FDR-adjusted p-values are computed with *Camera* (pre-ranked). **f** Heatmap of ChIP-seq signals around TSS regions (+/- 4kb) at which ZMYND11 bindings were identified by peak calling procedure (Macs2) in VCaP cells overexpressing the indication constructs. **g** IGV-derived screenshots representing loglikelihood ratio of ZMYND11 bindings in mutant SPOP (SPOP-Y87C) vs wild-type SPOP over-expressing VCaP cells. Reported are *MYC* (up) and *CDKN1A* (bottom). All error bars, mean ± s.e.m. *P* values were determined by two-way ANOVA (**b**) or one-way ANOVA with multiple comparisons and adjusted using Benjamini-Hochberg post-test (**c**). $^{**}P < 0.01$, $^{***}P < 0.001$. Molecular weights are indicated in kilodaltons (kDa).

Figure 6

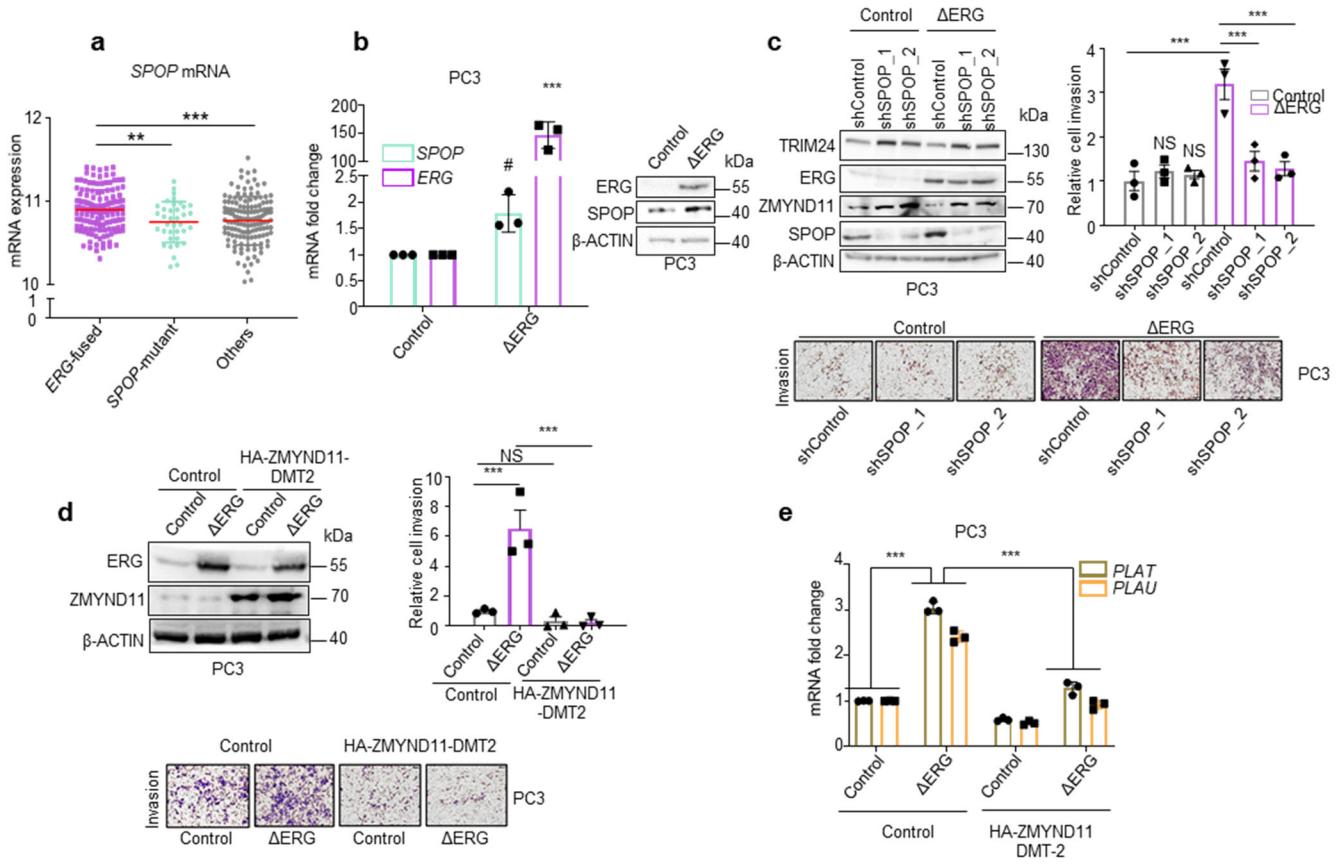

Fig. 6 SPOP-WT is an ERG target gene and required for ERG-mediated cell invasion. **a** *SPOP* mRNA expression levels in 333 primary prostate cancer tissues stratified according to the indicated driver mutations[1]. Error bars, mean ± s.d. **b** SPOP mRNA and protein levels in response to forced expression of ΔERG in PC3 prostate cancer cells by qPCR and immunoblotting, respectively. Error bars, mean + s.e.m. (n=3). *P* values were determined by unpaired, two-tailed Student's t-test. $^{\#}P < 0.05$; Control versus ΔERG for *SPOP* expression levels. $^{***}P < 0.001$; Control versus ΔERG for *ERG* expression levels. **c** Transwell Matrigel invasion assay of PC3 cells with forced expression of ΔERG and knockdown of SPOP using two different short hairpin RNAs. Protein expression of the indicated proteins was assessed in parallel by immunoblotting. Error bars, mean ± s.e.m. (n=3). **d** Transwell Matrigel invasion assay of PC3 cells with forced expression of ΔERG and HA-ZMYND11-DMT2 and corresponding immunoblot analysis. Error bars, mean ± s.e.m. (n=3). **e** Analysis of the ΔERG- and HA-ZMYND11-DMT2-induced transcriptional changes in the ERG target genes *PLAU* and *PLAT*. All error bars, mean ± s.e.m. *P* values were determined by one-way ANOVA with multiple comparisons and adjusted using Benjamini-Hochberg post-test (**a,c,d,e**). NS, not significant. $^{**}P < 0.01$, $^{***}P < 0.001$. Molecular weights are indicated in kilodaltons (kDa).

Figure 7

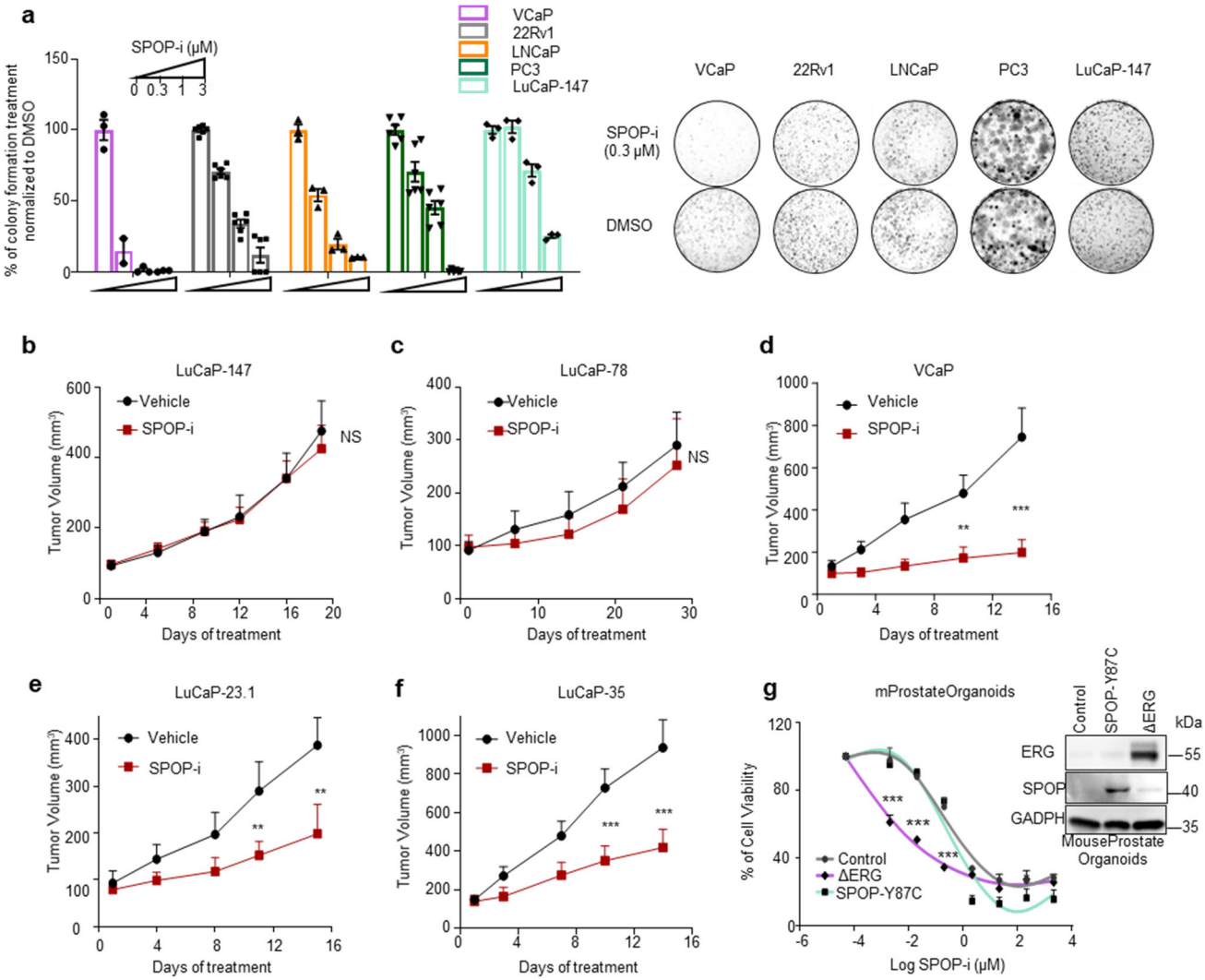

Fig. 7 *ERG*-positive tumor cells are particularly sensitive to SPOP inhibition. **a** SPOP inhibitor (SPOP-i, compound 6b) mediated 3D growth inhibition in methylcellulose in the indicated prostate cancer cell lines. **b** Tumor growth kinetics with (n =10) or without (vehicle; n = 10) SPOP-i treatment in xenografts established from LuCaP-147 (SPOP-Y83C) PDX cells. **c** Tumor growth kinetics with (n = 4) or without (vehicle; n = 4) SPOP-i treatment in xenografts established from LuCaP-78 (SPOP-W131G) PDX cells. **d** Tumor growth kinetics with (n = 11) or without (vehicle; n = 11) SPOP-i treatment in xenografts established from VCaP. **e** Tumor growth kinetics with (n = 8) or without (vehicle; n = 10) SPOP-i treatment in LuCaP-35 (ERG-positive) PDX. **f** Tumor growth kinetics with (n = 6) or without (vehicle; n = 8) SPOP-i treatment in LuCaP-23.1 (ERG-positive) PDX. All SPOP-i treatment initiated when tumors reached an average of $100mm^3$. **g** Dose-response curves to SPOP-i treatment of Mouse Prostate Organoids overexpressing ΔERG, SPOP-Y87C and Control vector**.** All error bars, mean + s.e.m. *P* values were determined by two-way ANOVA with multiple comparisons and adjusted using Benjamini-Hochberg post-test. NS, not significant. $^{**}P < 0.01$, $^{***}P < 0.001$.

Figure 8

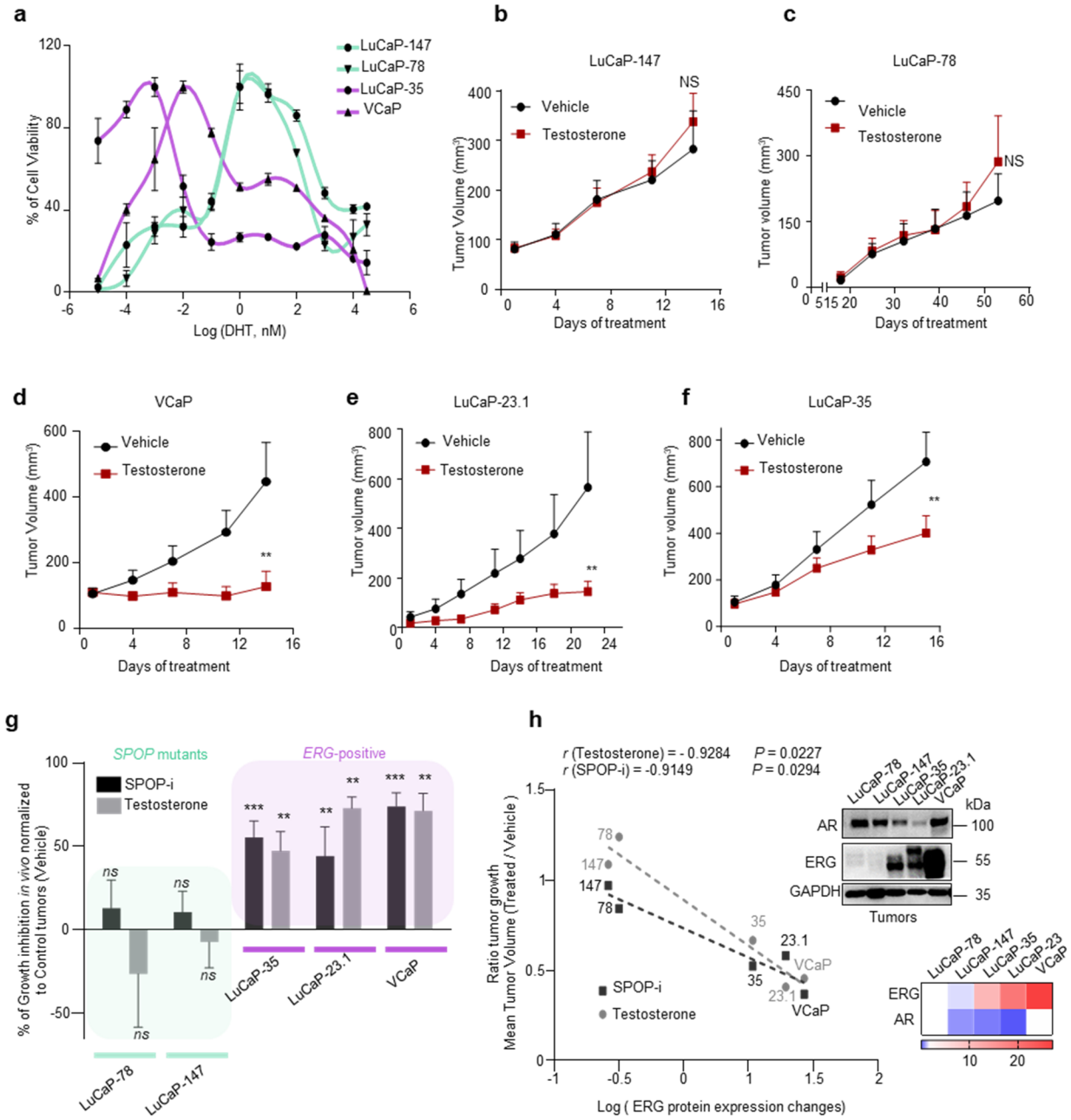

Fig. 8 ERG and mutant SPOP trigger different responses to therapeutic interventions **a** Dose-response curves to DHT treatment of VCaP, LuCaP-35, LuCaP-78 and LuCaP-147 PDX cancer cells. Prior to DHT treatment, PDX were grown in standard media without DHT. VCaP were starved for 24h in CSS medium (RPMI + 10% charcoal-stripped serum). Cell viability was assessed after 2 weeks. **b** Tumor growth kinetics with (n = 10) or without (vehicle; n = 10) testosterone treatment in xenografts established from LuCaP-147 (SPOP-Y83C). **c** Tumor growth kinetics with (n = 4) or without (vehicle; n = 4) testosterone treatment in xenografts established from LuCaP-78 (SPOP-W131G) cells. **d** Tumor growth kinetics with (n = 6) or without (vehicle; n = 10) testosterone treatment in xenografts

established from VCaP (ERG positive) cells. **e** Tumor growth kinetics with (n =12) or without (vehicle; n = 12) testosterone treatment in xenografts established from LuCaP-23.1 (ERG positive) cells. **f** Tumor growth kinetics with (n = 10) or without (vehicle; n = 10) testosterone treatment in xenografts established from LuCaP-35 (ERG positive) cells. **g** Sensitivity to Testosterone and SPOP-i treatment in xenograft and PDX models. LuCaP-23.1, LuCaP-35 and VCaP are *ERG*-positive cancer cells. LuCaP-147 and LuCaP-78 are *SPOP* mutant cancer cells (respectively SPOP-Y83C and SPOP-W131G). Growth inhibition is calculated using the last tumor measurements as shown in b-f and Fig. 7b-f. **h** Correlation of sensitivity to SPOP-i or testosterone treatment shown in Extended Data Fig. 8f-j and 9e-i, with ERG protein levels, as quantified by immunoblot, in PDX models and xenografts. *P* values were calculated using Pearson rank correlation. Corresponding immunoblot and quantification of AR and ERG protein levels depicted as a heatmap. Protein expression changes were normalized to GAPDH and LuCaP-78. All error bars, mean + s.e.m. *P* values were determined by two-way ANOVA with multiple comparisons and adjusted using Benjamini-Hochberg post-test (**b-e**) or by unpaired, two-tailed Student's t-test (**g**), NS, not significant. $^{**}P < 0.01$, $^{***}P < 0.001$. Molecular weights are indicated in kilodaltons (kDa).

Figure 9

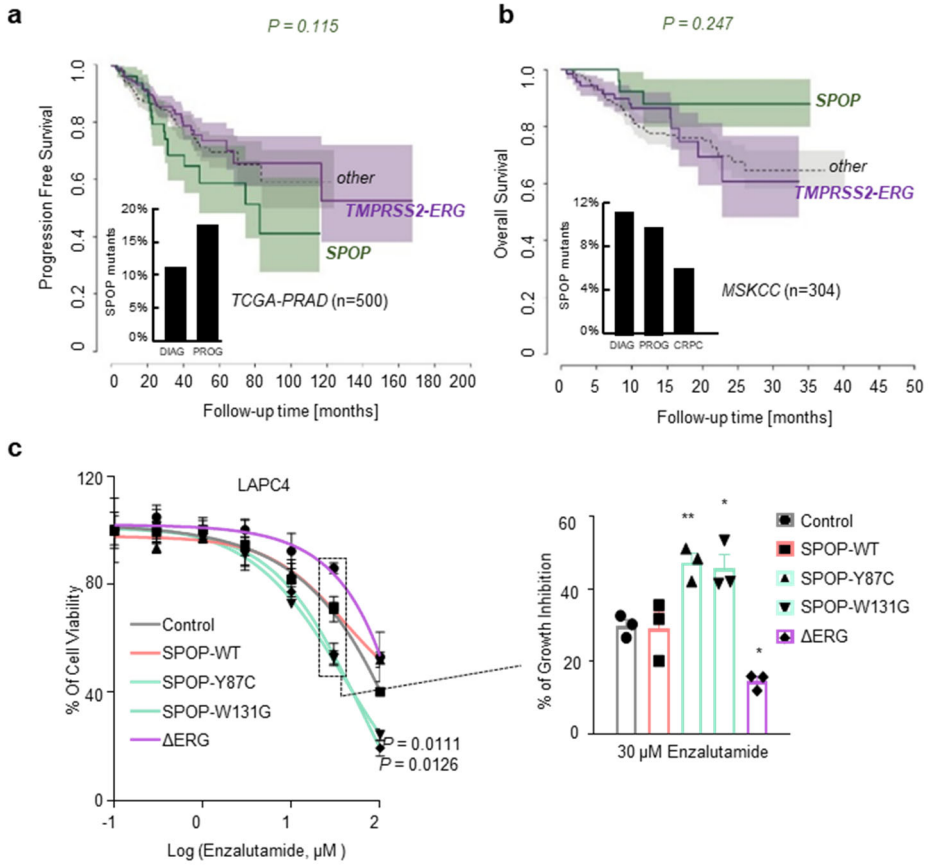

Fig. 9 *SPOP* mutant tumors are particularly susceptible to androgen deprivation therapies (ADT). a Progression-free survival of prostate cancer patients derived from the TCGA-cohort. Curves representing TMPRSS2-ERG rearranged and SPOP-mutant patients are indicated in violet and green, respectively. The area around the curves represents 80% confidence interval. The bar plot in the lower left corner indicates the percentage of SPOP-mutant tumors within all patients who were diagnosed with prostate cancer (DIAG) and within the individuals who developed a progression of the disease (PROG). **b** Overall survival of prostate cancer patients derived from the MSK-IMPACT cohort. Curves representing *TMPRSS2-ERG* rearranged and *SPOP*-mutant patients are indicated in violet and green, respectively. The area around the curves represents 80% confidence interval. The bar plot in the lower left corner indicates the percentage of SPOP-mutant tumors within all patients who were diagnosed with prostate cancer (DIAG), within individuals who developed a metastatic progression of the disease (PROG), and within individuals who developed castration-resistant prostate cancer (CRPC). P values for Kaplan-Meier curves were determined using log-rank test. **c** Enzalutamide sensitivity of LAPC4 cells overexpressing ΔERG or SPOP mutant species (Y87C, W131G). All error bars, mean + s.e.m. *P* values were determined by unpaired, two-tailed Student's t-test (**c**), NS, not significant. $*P < 0.05$, $**P < 0.01$. Molecular weights are indicated in kilodaltons (kDa).

Figure 10

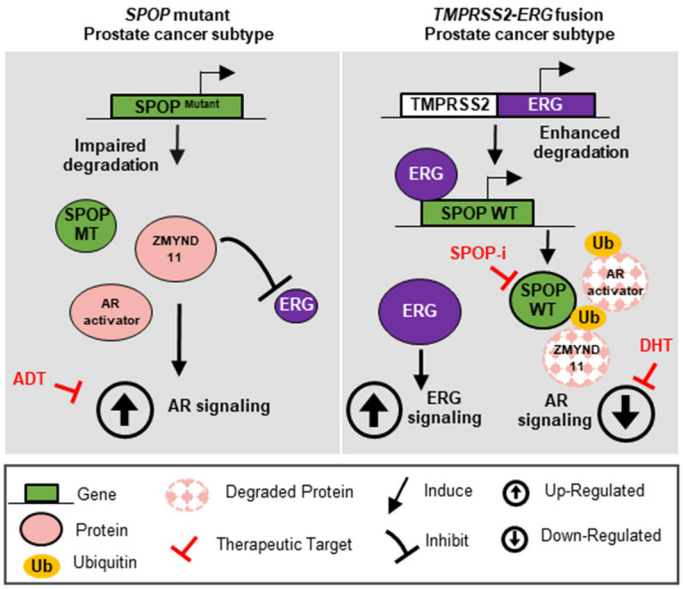

Fig. 10 Schematic representation of the proposed model for the aversive relationship between mutant *SPOP* and *ERG* in prostate cancer.

References

1 TCGA. The Molecular Taxonomy of Primary Prostate Cancer. *Cell* **163**, 1011-1025, doi:10.1016/j.cell.2015.10.025 (2015).